

The Impact of micro-tunnelling on adjacent pile foundations

Numerical modelling of micro-tunnel
excavation in PLAXIS

By

Yao Wang

to obtain the degree of

Master of Science
in Geo-Engineering

at the Delft University of Technology,

Student number: 4742869
Project duration: January 2019 – October 2019
Thesis committee: Dr. ir. W. Broere, TU Delft, chairman
Ir. K.J. Reinders, TU Delft
Ir. R. de Nijs, TU Delft

Abstract

A series of finite element simulations via PLAXIS were carried out to investigate the effects of micro-tunnelling on nearby pile foundations. A numerical model concerning the large diameter tunnel boring machine was first established based on identical properties of the centrifuge experiment executed by Loganathan et al. (2000). Results from numerical simulation were validated by measured data from the centrifuge test. After the validation of the numerical modelling method, the model was adjusted to match the case of micro-tunnel and a new model regarding the micro-tunnelling procedure was generated based on geotechnical conditions of the North/South Metro Line Amsterdam. The Hardening Soil constitutive model was chosen for all soil layers. In the model, the condition of single bored pile with working load was activated in the greenfield condition before the simulation of micro-tunnel. Advancement procedure of the micro-tunnel was simulated, and pile responses were collected under the plane strain condition. Based on the study of the model, two load transfer mechanisms of piles during tunnel-pile interaction process were identified. Impact of tunnel advancement on adjacent piles was also interpreted. A set of parametric studies were implemented to study changes of pile settlement and bearing capacity with increasing volume loss. An influence zone around the micro-tunnel respecting the potential of pile critical movements was established. Although the lack of field data makes the validation of results hard, comparison with analytical prediction and measured data from the centrifuge test shows good agreements for soil movements and pile responses. The results of this research remain to be validated by field data but it can provide insights into the problem of the impact of micro-tunnelling on piles.

Acknowledgements

I would like to express my gratitude to Wout Broere, Kristina Reinders and Richard de Nijs for their expert guidance and supervision during my graduation project.

Last but not least, I am very grateful to my parents and friends for their constant encouragement and support throughout my studies.

Delft, University of Technology
October 2019

Yao Wang

Table of Contents

1	INTRODUCTION	1
1.1	Background	1
1.2	Objectives of research	1
1.2.1	What are the mechanisms of interaction between pile and micro-tunnel?.....	1
1.2.2	How does the configuration between micro-tunnel and adjacent piles influence the pile responses?.....	1
1.2.3	How do piles respond concerning different volume loss of micro-tunnel excavation?	2
1.2.4	What is the impact of micro-tunnelling on bearing capacity of the pile?	2
1.3	Research Methods	2
1.3.1	Comparison between the centrifuge model and the numerical model	2
1.3.2	Two theoretical models regarding to the configuration	2
1.3.3	Parametric studies	2
2	LITERATURE REVIEW	3
2.1	Introduction.....	3
2.2	Pile responses caused by tunnelling: Physical observations.....	3
2.2.1	Full-scale field trials	3
2.2.2	Case histories.....	3
2.2.3	Centrifuge tests.....	4
2.3	Pile responses caused by tunnelling: Prediction methods	5
2.3.1	Numerical modelling.....	5
2.3.2	Empirical methods	6
2.3.3	Analytical methods	6
2.4	Current understanding of the problem.....	7
2.4.1	Load transfer mechanisms.....	7
2.4.2	Pile settlement.....	7
2.4.3	Pile axial force	8
2.4.4	Pile bending moment	8
2.5	Influence zone	8
2.5.1	Shear surface	8
2.5.2	Normalized pile head settlement	9
2.5.3	Pile settlement.....	10
2.5.4	Allowable settlements for buildings	11
2.6	Pipe-jacking technique.....	12
2.7	Full-scale trial of pipe-jacking	12

2.8	Soil models.....	13
2.8.1	The Mohr-Coulomb Model	13
2.8.2	The Hardening Soil Model	13
3	VALIDATION OF NUMERICAL MODELLING METHOD.....	14
3.1	Model Geometry	14
3.2	Constitutive Model and Model Parameters	16
3.3	Mesh generation	17
3.4	Numerical modelling procedures	17
3.5	Comparison of results between the centrifuge test and the numerical model	18
3.5.1	Surface settlement.....	18
3.5.2	Soil lateral movement & Pile lateral movement.....	19
3.5.3	Pile head settlement & relative settlement at the tip.....	21
3.6	Conclusions regarding the reliability of the numerical modelling method	21
4	DETAILS OF THE NUMERICAL MODELLING PROCEDURE.....	22
4.1	Ground conditions and soil profile	22
4.2	Material constitutive models	23
4.3	Micro-tunnelling parameters for analysis	23
4.3.1	Properties of micro-tunnel boring machine.....	23
4.3.2	The shape of the MTBM shield	24
4.3.3	Tunnel face stability.....	25
4.3.4	Overburden pressure of soil	26
4.3.5	Lubrication and soil convergence	26
4.3.6	Volume loss	26
4.3.7	Lining	27
4.3.8	Summary of properties	27
4.4	Pile parameters for analysis	28
4.4.1	Properties of the bored concrete pile	28
4.4.2	Shaft resistance of pile	28
4.4.3	Base resistance of pile.....	29
4.5	Mesh generation	30
4.6	Modelling of phased excavation	30
5	MODELS SIMULATED IN PLAXIS 3D.....	32
5.1	Pile load test.....	32
5.2	Deep tunnel condition.....	34
5.2.1	Geometry	34
5.2.2	MTBM advancement	34
5.2.3	Pile responses induced by tunnelling	35

5.3	Shallow tunnel.....	38
5.3.1	Geometry.....	38
5.3.2	Pile responses due to tunnelling	38
5.4	Different failure mechanisms of deep and shallow tunnelling models	42
6	PARAMETRIC STUDY	43
6.1	Influence zone	43
6.1.1	Pile responses at volume loss of 3%	45
6.1.2	Pile responses at volume loss of 9%	49
6.1.3	Pile responses at volume loss of 15%	51
6.1.4	Influence zone in the vertical direction.....	53
6.1.5	Influence zone of micro-tunnel.....	53
6.2	The impact of micro-tunnelling on bearing capacity of the pile.....	55
6.2.1	The change of bearing load during the MTBM advancement procedure	55
6.2.2	The changes in bearing loads with increasing volume loss	56
7	CONCLUSIONS.....	58
7.1	Deep and shallow tunnelling models.....	58
7.2	Influence zone of micro-tunnel	58
8	REFERENCE	59

List of Figures

Figure 1. Influence zone defined by shear surface	9
Figure 2. Influence zone built on full-scale trials proposed by Kaalberg et al. (2005).....	10
Figure 3. Influence zone based on the relative settlement of pile proposed by Selemetas et al. (2005)	10
Figure 4. Influence zone based on large pile settlement proposed by Jacobsz et al. (2004).....	11
Figure 5. Influence zone based on an allowable settlement for building proposed by Vu et al. (2015)	11
Figure 6. Configuration of the London Clay model	15
Figure 7. Sketch of London Clay model in the longitudinal direction	15
Figure 8. Mesh of the model in PLAXIS 3D.....	17
Figure 9. Sketch of the advancement of the TBM	18
Figure 10. Surface settlement trough (a) numerical prediction in PLAXIS (b) measured and analytical results from Loganathan et al. (2000)	19
Figure 11. Soil lateral movement (a) numerical prediction in PLAXIS (b) measured and analytical results from Loganathan et al. (2000)	20
Figure 12. Pile lateral movement (a) numerical prediction in PLAXIS (b) measured and analytical results from Loganathan et al. (2000)	20
Figure 13. Sketch of soil profile based on the description of Delfgaauw et al. (2009)	22
Figure 14. Sketch of MTBM in the longitudinal direction	24
Figure 15. Pile head settlement with different pile head loads.....	33
Figure 16. Pile head settlement curve in the form of NEN9997-1+C2 (2017)	33
Figure 17. Sketch of the deep tunnel model.....	34
Figure 18. Sketch of the advancement of the MTBM model.....	35
Figure 19. Change of axial load of the pile in deep tunnel model.....	36
Figure 20. Change of Shaft friction of the pile in deep tunnel model	36
Figure 21. Change of pile tip settlement of the pile during deep MTBM advancement	37
Figure 22. Change of base load of the pile during deep MTBM advancement.....	38
Figure 23. Sketch of the configuration of the shallow tunnel model.....	38
Figure 24. Change of base load of the pile in the shallow tunnelling model	40
Figure 25. Change of shaft friction of the pile in the shallow tunnelling model.....	40
Figure 26. Bending moment of the pile due to tunnelling in the shallow tunnelling model.....	40
Figure 27. Lateral movement of the pile due to tunnelling in the shallow tunnelling model	40
Figure 28. Change of base load of the pile during shallow MTBM advancement	41
Figure 29. Change of pile tip settlement during shallow MTBM advancement	41
Figure 30. Influence zone proposed by Selemetas et al. (2005) based on pile head relative settlement	43
Figure 31. Locations of 19 pile toes.....	44
Figure 32. Changes of base loads of P4 – P19 with volume loss of 3%	46

Figure 33. The first boundary of the influence zone	46
Figure 34. Pile head settlements of P4-P19 with volume loss of 3%	47
Figure 35. Extensometer readings related to a reference value at Station-Rokin.....	48
Figure 36. Extensometer readings related to a reference value at Station-Ceintuurbaan	48
Figure 37. Variation of base loads of P4-P19 with volume loss of 9%	49
Figure 38. Pile head settlements of P4-P19 with volume loss of 9%	50
Figure 39. Pile head relative settlements of P4-P19 with volume loss of 9%	50
Figure 40. Changes of base loads of P4-P19 with volume loss of 15%	52
Figure 41. Three subdivided parts of the influence zone	52
Figure 42. Five pile tests to figure out the vertical boundary of the influence zone	53
Figure 43. Pile head relative settlements with increasing volume loss.....	54
Figure 44. An integrated influence zone of MTBM	54
Figure 45. Five pile bearing capacity tests	56
Figure 46. Changes of bearing loads with increasing volume loss.....	57

List of Tables

Table 1. Parameters of The Hardening Soil model.....	13
Table 2. Properties of The Mohr-Coulomb model used in the London Clay model	16
Table 3. Properties of the tunnel bored machine in London Clay model	16
Table 4. Properties of concrete, shield and pile.....	16
Table 5. Pile head settlement, lateral deflection and relative settlement	21
Table 6. Change of base load due to tunnelling.....	21
Table 7. Four soil layers and their properties in the model of MTBM	23
Table 8. MTBM properties.....	23
Table 9. Properties of MTBM shield and lining	24
Table 10. Length of sections of MTBM model	24
Table 11. Relationship between pressure ratio and volume loss	27
Table 12. Properties of MTBM model created in PLAXIS 3D.....	27
Table 13. Properties of the bored pile used in the MTBM model	28
Table 14. Beading capacities of piles with different lengths	29
Table 15. Initial settlements of piles with different lengths	32
Table 16. Pile head settlements with the increasing working load.....	33
Table 17. Parameters of the configuration of the deep tunnel model	34
Table 18. Test arrangement and test conditions	44
Table 19. Variations of bearing loads of 19 piles with volume loss of 3%	45
Table 20. pile head relative settlements of P4-P19 with volume loss of 3%	47
Table 21. Changes of base loads of 19 piles with volume loss of 9%	49
Table 22. Changes of base loads with volume loss of 15%	51

1 Introduction

1.1 Background

Micro-tunnelling for underground pipelines is gaining increasing popularity in heavily built-up cities due to its unparalleled advantage in terms of the trenchless method compared to the conventional pipe laying in trenches. Ground disturbance and damage to structures and services are significantly reduced and inconvenience to vehicular traffic and the public in general minimized. Extensive research has been implemented worldwide on the effects of tunnelling on nearby structures. However, very limited work has been reported about cases concerning micro-tunnelling. In this research, the prediction of pile responses due to the micro-tunnel excavation was given and interaction mechanisms between pile and micro-tunnel were demonstrated in detail based on literature studies and numerical modelling experiment. Although results of numerical modelling of the micro-tunnelling procedure cannot be validated directly by field data, it is expected these numerical simulations can provide insights into the problem and provide supports and data to researchers who work in this field in the future.

1.2 Objectives of research

The main question of this research is the impact of micro-tunnelling on adjacent pile foundations. To answer this question, it was split into several aspects:

1.2.1 What are the mechanisms of interaction between pile and micro-tunnel?

Analytical and numerical analyses of studies of large size TBM excavation are well-presented and the knowledge of the interaction between pile and TBM has been fully organized by previous researchers. The question is how to transfer the knowledge to case of the micro-tunnelling procedure and find the mechanisms of interaction between micro-tunnel and adjacent piles.

1.2.2 How does the configuration between micro-tunnel and adjacent piles influence the pile responses?

As one of the main factors that decide the responses of piles due to tunnelling activities, different configurations could result in absolute diverse responses of piles. Therefore, the impact of configuration was investigated to provide a solid foundation of understanding.

1.2.3 How do piles respond concerning different volume loss of micro-tunnel excavation?

Volume loss ratio is reported as another critical factor determining pile behaviour during the interaction process. Especially when a threshold value of volume loss has been exceeded, the pile failure is usually followed.

1.2.4 What is the impact of micro-tunnelling on bearing capacity of the pile?

Depending on different configurations between the micro-tunnel and the pile, load transfer mechanism of the pile can be variable, inducing different pile responses. In deep tunnelling and shallow tunnelling models discussed in this research, different patterns of variation of bearing capacity of the pile due to the stress relief were found.

1.3 Research Methods

Corresponding to research objectives, specific research methods were adopted and described below:

1.3.1 Comparison between the centrifuge model and the numerical model

To answer this question, the first model in PLAXIS 3D was built to simulate the centrifuge experiment carried by Loganathan et al. (2000) with identical properties. Results from numerical modelling validated by measured data of the centrifuge test. After the validation of the numerical modelling method, it was adjusted to fit the case of micro-tunnel. Results were interpreted from several aspects like ground settlement trough, pile load transfer mechanisms and pile failure mechanisms.

1.3.2 Two theoretical models regarding to the configuration

Following the way how it is studied in the cases of large diameter TBMs, two models with different load transfer mechanisms of pile concerning variable relative depths of the micro-tunnel regarding adjacent piles were established, which are called ‘deep tunnelling model’ and ‘shallow tunnelling model’ in this research. Changes in base resistance and shaft resistance due to micro-tunnelling procedure were illustrated and different failure criteria of piles were proposed based on different pile responses in two models

1.3.3 Parametric studies

Three groups of parametric studies with different volume loss ratios were conducted and pile responses concerning relative settlements and failure states were collected and interpreted. An influence zone respecting the potential of pile critical movement based on these studies was proposed.

2 Literature review

2.1 Introduction

Firstly, a review of the published literature on the effects of large diameter tunnel on nearby pile foundation is presented. Physical observations from case histories, field trials and centrifuge tests are introduced in Section 2.2. Prediction methods such as numerical approaches, analytical approaches and empirical methods are discussed in Section 2.3. Based on the study of literature, the understanding of the problem and critical questions is identified and discussed in Section 2.4. Considering the goal of this project, studies of the concept of ‘influence zone’ are highlighted in Section 2.5. A brief introduction of the technique about pipe-jacking is presented in Section 2.6. Since very restricted studies carried out on the impact of micro-tunnelling on adjacent structures, only one case study with instrumented ground movement caused by the excavation of micro-tunnelling was found and it will be introduced in Section 2.7. Section 2.8 gives a comparison of two soil constitutive models for numerical modelling.

2.2 Pile responses caused by tunnelling: Physical observations

2.2.1 Full-scale field trials

Kaalberg et al. (2005) conducted a full-scale trial test at the Second Heinenoordtunnel in the Netherlands to study the influence of tunnelling on piles and pile toes. The authors proposed that the impact of tunnelling on stress relieve of piles is almost negligible and an influence zone of the tunnel concerning different ratio between surface settlement and pile settlement was established. Besides, the difference between the inclination of predicted settlement trough and measured results was mentioned, which could also be found in subsequent studies.

Mair et al. (1993) and Lee (1994) reported the construction of a hand-dug escalator tunnel very close to pile foundation (1m clearance between tunnel and pile). The 1.2m diameter under-reamed bored piles were installed below the tunnel depth. Both in-ground and in-pile instrumentations were possible before tunnelling. Measurements of the in-pile inclinometers showed that the nearest pile was only subjected to maximum lateral deflection of 8mm for volume loss up to 2%. Besides, both the in-ground and in-pile inclinometers results were very similar. The authors concluded that tunnel could be constructed very close to pile foundation in London Clay and would only cause small horizontal deflection.

2.2.2 Case histories

Jacobsz et al. (2005) reported the monitoring of settlements of three piled-bridge foundations with one on end bearing piles and two on friction piles. These cases provide an opportunity for the predicted settlement to be compared with actual behaviour. Different mechanisms controlling the

behaviour of piles were applied to bored and friction piles, which will be discussed in detail later. The authors recommended that re-assessment of pile capacity should be carried out as a large factor of safety can often be found in piles and redistribution of loading is possible.

2.2.3 Centrifuge tests

Few case studies were installed with in-pile instrumentation. Therefore, some researchers resorted to centrifuge modelling technique which replicates realistic greenfield conditions and gives an accurate representation of the soil-structure interactions.

Loganathan et al. (2000) carried out three centrifuge tests with different tunnel-pile configurations in stiff clay to simulate the two-dimensional tunnelling-induced ground movement and pile responses. The greenfield soil movement, axial pile forces, pile settlements, and lateral pile deformations were measured and compared with analytical results. The author concluded that bending moment and lateral deflection of a pile is critical when tunnel spring line is located at or near the pile base and the axial force is critical for the pile when the tunnel spring line is below the pile base. Besides, a nearly linear relationship was observed between tunnelling induced maximum bending moments and ground loss values, which indicates that an elastic analysis of pile behaviour may be performed at volume loss less than 5% for similar soil-pile configurations to those used in this study.

Studies by Jacobsz et al. (2004) focused on the surface settlement and load distribution of single driven pile in dense sand with different volume loss caused by tunnel excavation. All the tests were carried out with the pile base above the tunnel. The zone of influence in which the large pile displacements could be expected was identified. For end-bearing piles, loads transfer from pile base to shaft gradually with the increase of volume loss and once maximum pile shaft capacity has been exceeded, large settlement occurs.

Marshall and Mair (2011) carried out a centrifuge test based on the study of Jacobsz et al. (2004) and considered the influence of the installation of piles before tunnel excavation. Authors claimed the installation of the driven piles significantly changed greenfield displacements, which means that analytical methods using greenfield displacements as an input to calculate pile responses are not appropriate for dealing with driven or jacked piles. Besides, the displacement data obtained during tunnel volume loss illustrated the mechanisms of soil displacement especially between pile base and tunnel crown. It is shown that strains resulting from pile-tunnel interaction could work to counteract greenfield soil strains, depending on the location of the pile.

Three centrifuge tests focus particularly on cases where the tunnels are modelled beneath or at the level of pile toes. Chiang and Lee (2007) implemented a group of centrifuge tests to investigate the responses of the single pile under various working loads to tunnelling in sandy ground. Pile responses under different tunnel embedded depths were measured and two different mechanisms of pile load transfer were proposed. Authors claim that only the depth ratio has a significant influence on the distributions of bending moments along with the piles, but both depth ratio and working load on the pile determine the profiles of the axial forces. Based on centrifuge results, authors deduced that the larger the working load on the existing pile before tunnelling, the larger the settlements that the pile experiences after tunnelling.

Cases mentioned above are both with driven piles. Mair and Williamson (2014) reported centrifuge model tests of the effects of tunnelling beneath bored piles in clay. The modelling showed that a single pile above the tunnel centerline settles more than the amount of surface settlement at the pile head. Only relatively small load redistribution was recorded, and pile failure did not occur even at high tunnel volume loss.

2.3 Pile responses caused by tunnelling: Prediction methods

2.3.1 Numerical modelling

Mroueh and Shahrour (2002) carried out a three-dimensional finite element modelling to study the influence of advancement of TBM to pile foundations. A simplified stress release zone was simulated to represent the effect of shield, over-cut and tail void grouting. No physical data was back-analyzed. The changes of pile responses i.e. axial forces, bending moment and deflection, during the excavation process were illustrated. The results showed that the impact of tunnelling on piles in the lateral direction is much larger than that in the longitudinal direction. Besides, soil movements with the existence of pile were compared with greenfield data and authors claimed that calculation with the greenfield soil movement is conservative. Considering that the influence of installation of the pile was not mentioned, which may weaken the soil around the pile, the conclusion still needs to be validated. Two different failure mechanisms due to configurations were also found in this study, verifying centrifuge test results of Loganathan et al. (2000).

A three-dimensional, elasto-plastic, coupled consolidation finite element analysis was conducted by Lee and Ng (2005) to investigate the influence of an advancing open face tunnel excavation on a nearby loaded pile. Experiment parameters in Loganathan et al. (2000)'s centrifuge test were adopted to build the numerical model. The study mainly focused on the interaction between tunnel and pile in advancing, i.e. longitudinal, direction. A zone of influence was identified one tunnel diameter ahead and one diameter behind the excavation face. Changes of surface and subsurface settlement, pore water pressure and pile responses with the advancing of the tunnel were illustrated. The results of bending moments in longitudinal and transverse directions were compared and were consistent with those from Mroueh and Shahrour (2002). Besides, plain strain surface and subsurface settlements were compared with results of centrifuge model and analytical predictions calculated by the given volume loss and shown similar trends.

Cheng et al. (2007) proposed a displacement-controlled method to simulate tunnelling process rather than simply removing forces corresponding to initial stress state, which tends to predict the wrong shape of ground displacement profile, hence wrong forces in piles. The DCM simulates tunnelling by applying displacement to the tunnel boundary and the suitability of it was demonstrated by back analysis of a centrifuge test and a field case study.

2.3.2 Empirical methods

In practice, the ground deformations are often described by empirical formulas based upon field observations. A normal (Gaussian) distribution curve proposed by Peck is used to predict the transverse settlement trough. Nevertheless, it has no theoretical basis.

The greenfield displacements at the pile base were used by Jacobsz et al. (2005) as the pile head settlement to simplify the problem. Such approaches are usually conservative for displacements of the pile tip. Besides, empirical methods are subject to some limitations, such as their application of different tunnel geometries, ground conditions, construction techniques, and the limited information they provide about the subsurface settlement.

2.3.3 Analytical methods

Loganathan and Poulos (1998) proposed an analytical method redefining the traditional ground loss parameter concerning the gap parameter proposed by Lee et al. (1992) and incorporated the equivalent ground loss parameter into the closed-form elastic solutions derived by Verruijt and Booker (1998). The new method provides predictions of tunnel-induced surface and subsurface settlements and horizontal movements in clays. The applicability of the proposed method was evaluated by a back analysis of five case studies. The settlement troughs predicted are slightly wider than those observed or estimated using empirical methods. Nevertheless, good agreements have been illustrated for subsurface and horizontal soil movements for uniform clay profiles.

Chen et al. (1999) used a two-stage approach method to analyze the lateral and axial responses of a single pile. In the first stage, greenfield soil movements were calculated from the analytical method proposed by Loganathan and Poulos (1998). In the second stage, the computed soil movements were imposed on boundary element analyses to compute the pile responses. Simply design charts were established by parametric studies and were validated by a back analysis of a case history. However, simply imposing greenfield displacements to piles ignores the influence of the installation of piles before tunnel excavation. The differences between these two methods were illustrated by Marshall and Mair (2011) but details still need to be investigated further.

2.4 Current understanding of the problem

This section presents the comparison of all the reported field observation and tries to find some similarities in their results to understand the pile responses to tunnelling. The following sign conventions for the bending moment and the axial force are used: the compressive axial forces are taken as positive, and the bending moments are treated as positive if they act to bend the pile away from the tunnel. It should be noted that piles mentioned in summaries below are both with working loads.

2.4.1 Load transfer mechanisms

Centrifuge tests reveal that tunnel-pile configuration has a significant influence on pile responses. Two typical situations are encountered in practice: (a) tunnelling under pile tip, i.e. deep tunnelling and (b) tunnelling adjacent to or above pile tip, i.e. shallow tunnelling and they develop different load transfer mechanisms before failure state.

When the tunnel is constructed at the level of or under the pile tip, the pile base resistance will be first reduced due to stress relief of tunnelling. To fulfil the equilibrium of loads, the base resistance is transferred to the pile shaft so that positive skin friction along the pile increases. If the extra positive skin friction cannot compensate for the unavoidable large degradation of end bearing capacity, a larger pile settlement would be anticipated. Besides, the pile lateral response is unlikely to be of significance in this situation.

In the second situation where the tunnel is constructed above or some distance far from the pile tip, a different mechanism is observed. The stress relief due to tunnelling causes negative skin friction to act along the pile shaft above the tunnel level. To maintain the equilibrium, the pile shaft below tunnel level (which can be seen as a fixed end) would support the drag-load from the upper part so that positive skin friction increases. Only when the positive shaft resistance and pile base are fully mobilized, the settlement would become a problem. Compared to the potential pile settlement, the lateral pile response can be significant since horizontal soil movement is the biggest near the tunnel.

2.4.2 Pile settlement

Pile settlement mainly depends on the depth ratio of tunnel and pile, i.e. L_p/H_{tunnel} , where L_p is the length of the pile and H_{tunnel} is the embedded depth of tunnel axis. The definitions of deep tunnelling and shallow tunnelling in previous part correspond to depth ratios of $L_p/H_{\text{tunnel}} \leq 1$ and $L_p/H_{\text{tunnel}} > 1$, respectively. Chung reported that the large pile settlement may be the concern only when $L_p/H_{\text{tunnel}} \leq 1$. For that, Jacobsz et al. (2004), Kaalberg et al. (2005) and Selemetas et al. (2005) have defined their own but similar zones of influence when pile tip is located above or near the tunnel. More description about the influence zone will be given later. The ratios between the pile settlement and the surface settlement are different depending on the position of pile tip in zones. Besides, it is also found by Lee & Ng that the pile settlement is significant if the pile-tunnel clearance in the longitudinal direction is less than one tunnel diameter.

2.4.3 Pile axial force

Chiang and Lee (2007) illustrated detailed load transfer mechanisms for shallow tunnelling, i.e. $L_p/H_{\text{tunnel}} > 1$ and deep tunnelling, i.e. $L_p/H_{\text{tunnel}} \leq 1$. The author reported that pile axial force is maximum at tunnel springline level when $L_p/H_{\text{tunnel}} > 1$ and at pile head level when $L_p/H_{\text{tunnel}} \leq 1$. This trend agrees with centrifuge test results from Loganathan et al. (2000).

2.4.4 Pile bending moment

In the study of Chiang and Lee (2007), the pile with pile tip far below the tunnel horizontal axis were found to have both positive and negative bending moments for the upper and lower portions of the pile, respectively, because the lower portions of the pile behave like a fixed end. For the case of $L_p/H_{\text{tunnel}} \leq 1$, a negative bending moment developed along the full length of the pile. The lower portions of the pile behave like a free end in this situation.

Most of the studies have been focusing on transverse bending moment due to the simulation of plane strain tunnel. Mroueh and Shahrour (2002) simulated the 3D tunnel advancement and showed that the transverse bending moment is nearly 3 times larger than the longitudinal bending moment. This conclusion was also verified by Lee and Ng (2005).

2.5 Influence zone

Influence zone is widely used in engineering practice as a guideline to control tunnel position concerning adjacent pile foundations. Lots of researchers established specific influence zones based on different criteria including typical shear surface, pile settlement, normalized pile head settlement and building settlement. These criteria are summarized and evaluated below.

2.5.1 Shear surface

Figure 1 shows that influence zone defined by a β line with an angle of $\beta = 45^\circ - \phi'/2$ to the vertical where ϕ' is the effective friction angle of the soil. This β line extending from the tunnel boundary to the ground surface is based on the typical shear surface first proposed from model test results by Morton and King (1979). After that, the shear surface was connected with a wedge of width $\pm 2.5i$ at the ground beginning from the tunnel lining proposed by Attewell et al. (1986), where i is the distance from the tunnel central line to the point of inflection.

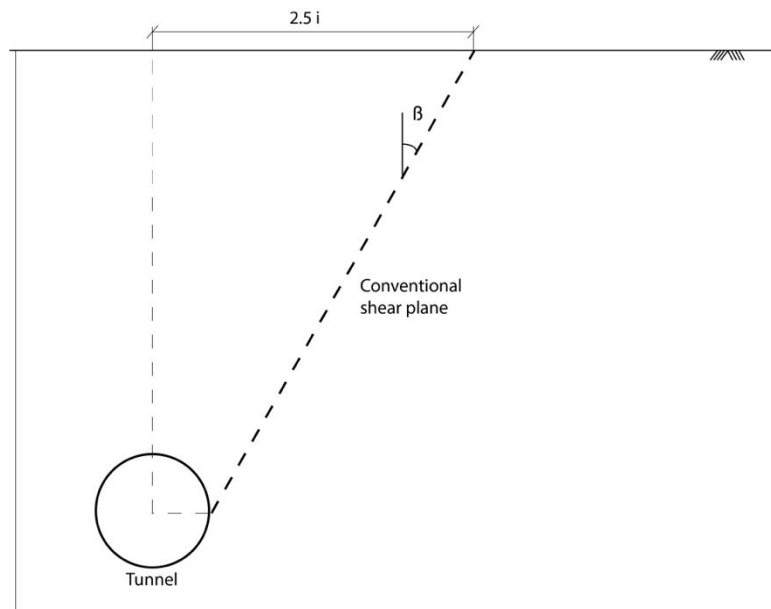


Figure 1. Influence zone defined by shear surface

2.5.2 Normalized pile head settlement

Kaalberg et al. (2005) conducted the Heinenoord full-scale trial near Rotterdam, in which the response of 38 timber piles and 18 concrete piles was monitored during the construction of 8.3 m diameter twin tunnels through both Holocene deposits (layers of soft clay and peat) and Pleistocene dense sand. Field measured data showed that piles located near the tunnel could be classified into three categories as shown in Figure 2. Piles with their bases in Zone A settled more than the ground surface, piles in Zones B settled approximately by the same amount as the ground surface and piles founded in Zones C settled less than the ground surface.

Based on the research of Kaalberg et al. (2005), Selemetas et al. (2005) conducted a full-scale trial during the construction of the new Channel Tunnel Rail Link (CTRL) in the UK and three zones of influence were identified in which pile head settlements were correlated to surface ground settlements.

As shown in Figure 3, the parameter R is defined as the ratio between pile head settlement and surface ground settlement. Compared with the results of Kaalberg et al. (2005), Selemetas et al. (2005) gave a more specific description of the pile settlements in the zone. Piles in Zone A settled 2-4 mm more than the ground surface. Piles in Zone B settled by the same amount as the ground surface and Piles in Zone C settled less than the ground.

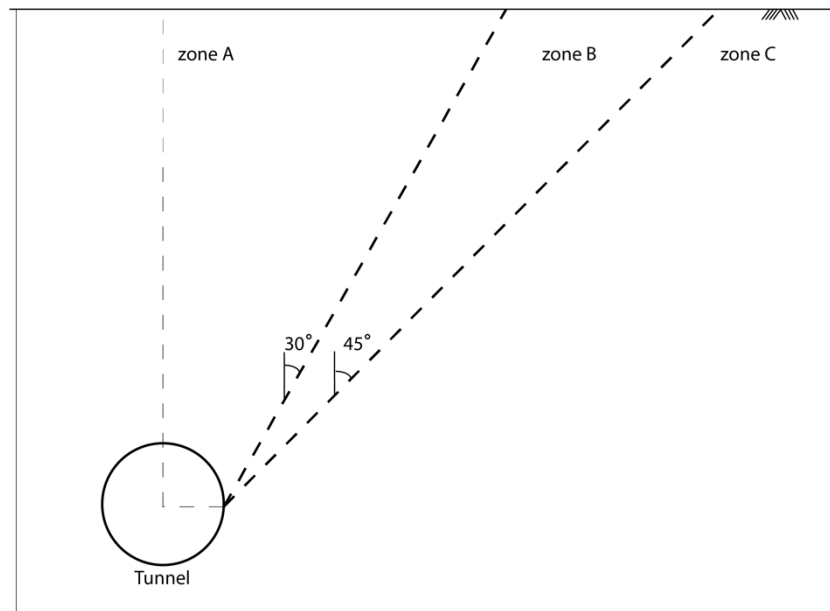


Figure 2. Influence zone built on full-scale trials proposed by Kaalberg et al. (2005)

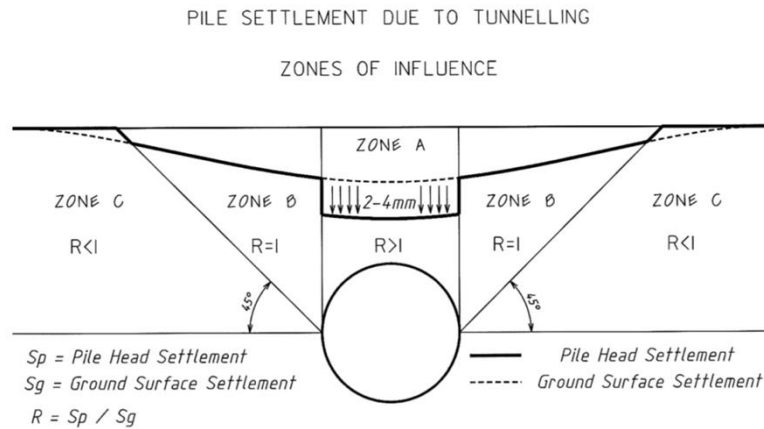


Figure 3. Influence zone based on the relative settlement of pile proposed by Selemetas et al. (2005)

2.5.3 Pile settlement

Jacobsz et al. (2004) conducted a parametric study in centrifuge model with single axial loaded piles driven in dry sand and similar zones of influence were established. The settlements of piles located at different positions concerning the tunnel revealed a roughly parabolic-shaped zone of influence as shown in Figure 4. A criterion was chosen regarding the potential for a large settlement, namely 20 mm at prototype scale, exists at volume loss greater than 1.5%. Inside the zone, it was divided further by several lines according to the settlement of piles at volume loss of 1.5% compared with the surface settlement.

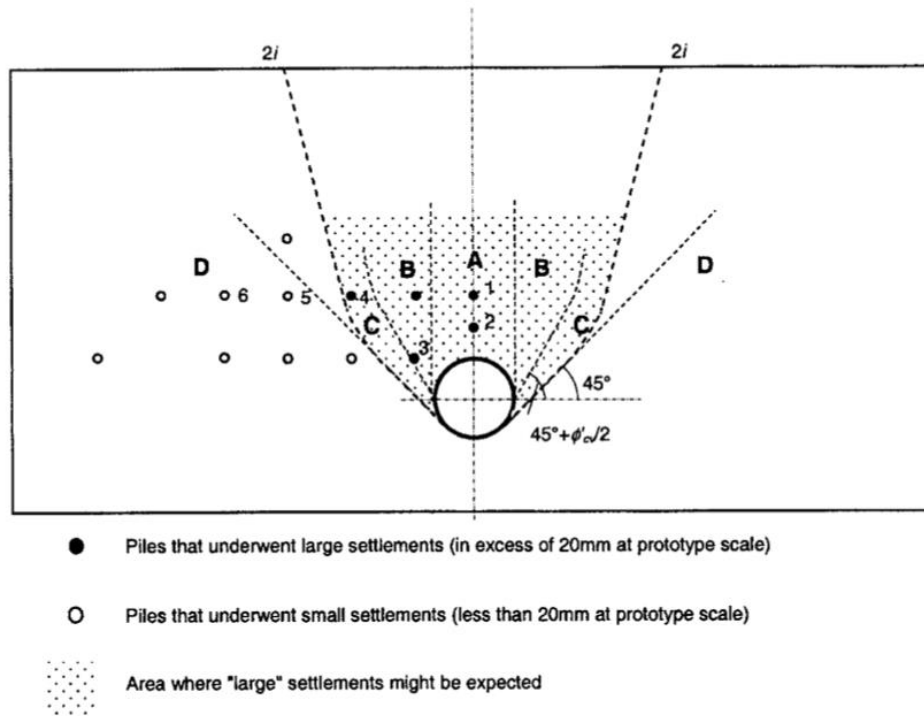


Figure 4. Influence zone based on large pile settlement proposed by Jacobsz et al. (2004)

2.5.4 Allowable settlements for buildings

Unlike the definition of influence zone given by Jacobsz et al. (2004), Vu et al. (2015) established the influence zone due to tunnelling from the aspect of allowable settlement u_{\max} and slope ω_{\max} for the buildings on the ground surface. The comparison with the results from Kaalberg et al. (2005) was illustrated in Figure 5. The area where $u_{\max}/V_L \geq 0.4m$ corresponds to Zone A in the study of Kaalberg et al. (2005) and the area with $0.04m \leq u_{\max}/V_L \leq 0.4m$ overlaps Zone B.

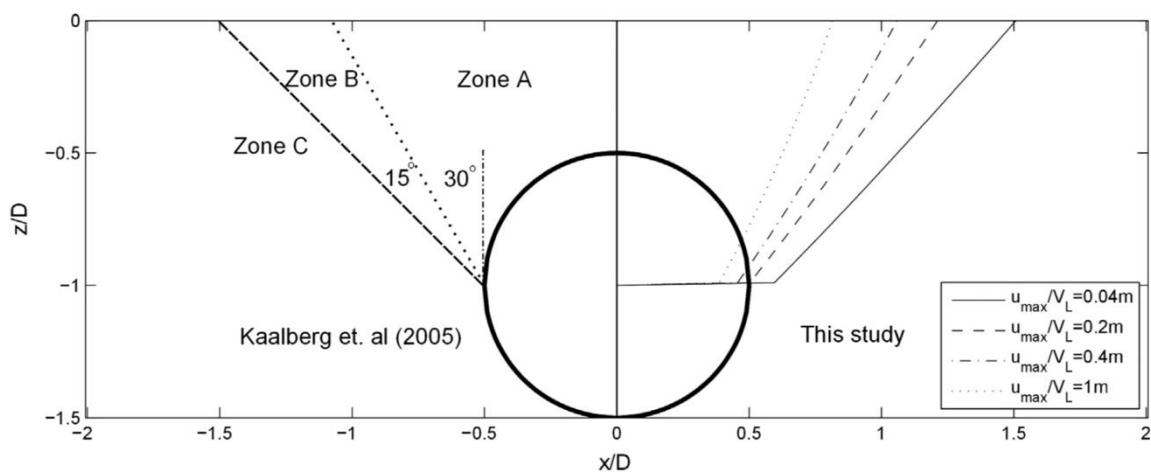


Figure 5. Influence zone based on an allowable settlement for building proposed by Vu et al. (2015)

2.6 Pipe-jacking technique

This section briefly introduces techniques of pipe jacking and micro-tunnelling. The term micro-tunnelling is used to describe the technique of using a tunnelling machine in combination with pipejacking. Internal diameters of jacked-pipe are normally between about 0.9 and 3.0 meters. Pipe jacking with diameter less than 900 mm is usually referred to as micro-tunnelling.

During the pipe jacking, pipes are pushed through the ground using hydraulic jacks from a thrust pit to a receiving pit. Excavation takes place at the front end by method ranging from hand excavation with a shield to full-face tunnel boring machines. In the less stable ground, slurry or earth pressure balance tunnel boring machines may be used. Micro-tunnelling systems are essentially miniaturized versions of pipe jacks using full-face tunnelling machines. At the thrust pit, the jacking force is usually provided by two or four hydraulic rams. The ram loads are distributed onto the end of the pipe being jacked through a substantial thrust ring. The ram loads are supported by a thrust wall at the back of the jacking pit, transferring the loads to the ground.

The pipes used in pipe jacking may be manufactured in various materials, including reinforced or unreinforced concrete, steel, ductile iron, glass-reinforced plastic or vitrified clay. For large diameters, reinforced concrete is commonly used. Standard pipes in large diameters are typically 2.5m long. The maximum pipe length that can be jacked depends on ground conditions, size and strength of pipes, type of shield and other factors. Roughly 80 m for micro-tunnelling and up to about 150 m for large diameter pipe jacks are commonly achieved. Length can be greatly increased by the application of lubrication and by incorporation of intermediate jacking stations. Jacking stations are steel cylinders containing a set of jacks which create a telescopic joint within the pipeline. Although the theoretical length of pipe could be infinite using intermediate stations, economic lengths for machine drives are common of the order of 300-400 m.

The technique has several potential advantages over other methods of installing pipes and small diameter tunnels as listed below:

1. Strong, rigid lining installed immediately after excavation;
2. The completely enclosed operation for safe working in the unstable ground;
3. Ground movement controlled;
4. High-quality internal finish without the need for secondary lining.

2.7 Full-scale trial of pipe-jacking

Very few case studies were reported about the interaction between micro-tunnelling and surrounding soil. The only one instrumented case history was carried out by Marshall (1998).

On-site monitoring of full-scale pipe jacks in four different ground conditions was conducted. In each scheme, the displacements around the tunnel and ground pressure were measured. The ground movements were measured using conventional surveying techniques for surface settlement and inclinometer access tubes for sub-surface deformation. The measured data were compared to results from empirical predictive methods and showed that short-term displacements are related to ground losses caused by the closure of the over-break void between shield and pipe.

2.8 Soil models

2.8.1 The Mohr-Coulomb Model

The Mohr-Coulomb (MC) Model is a linear elastic perfectly plastic model in which no hardening or softening occurs. The elastic part of the model is established on Hooke's law of isotropic elasticity and the perfectly-plastic part is based on the Mohr-Coulomb failure criterion in a non-associated plasticity framework. To evaluate the occurrence of plasticity, a yield function, f , is introduced where plastic yielding is represented by $f = 0$. The yield surface in this perfectly-plastic model is fully defined by model parameters and not changed with plastic straining. Within the yield surface, the pure elastic and reversible strains occur and plasticity with irreversible strain occur outside the surface.

Since the simplicity of the Mohr-Coulomb model, it is usually used as a first approximation of soil behaviour. Mroueh and Shahrour (2002) used it to simulate soil behaviour in the process of tunnel excavation. Research indicated that the Mohr-Coulomb model could provide rough estimation for surface settlement trough and subsurface movement of soil but poorly performed in simulating complex geotechnical conditions. For that situation, a more advanced constitutive model is usually required.

2.8.2 The Hardening Soil Model

The Hardening Soil (HS) Model is an advanced model to simulate soil behaviour, for both soft soils and stiff soils (Schanz et al., 1999). Unlike elastic perfectly-plastic models, the yield surface of a hardening plasticity model is not fixed but able to expand because of plastic strain. The HS model includes an isotropic, compression hardening cap yield surface, a shear hardening yield surface and the MC failure criterion. The cap yield gives a better prediction of the development of plastic strains in isotropic and oedometer loading and the shear yield concerns the evolution of plastic strains due to deviatoric loading. The MC criterion forms the boundary of failure as a function of the shear strength of the material. Some basic parameters of the model are:

Table 1. Parameters of The Hardening Soil model

E_{50}^{ref}	Secant stiffness in standard drained triaxial test
$E_{\text{ode}}^{\text{ref}}$	Tangent stiffness for primary oedometer loading
$E_{\text{ur}}^{\text{ref}}$	Unloading/reloading stiffness
m	Power for stress-level dependency of stiffness
c, φ, ψ	Cohesion, friction angle and dilation angle for the MC failure criterion

E_{50}^{ref} concerns the plastic strain caused by primary deviatoric loading; $E_{\text{ode}}^{\text{ref}}$ is used to describe the plastic strain due to primary compression; $E_{\text{ur}}^{\text{ref}}$ is the unloading / reloading stiffness and the default value in Brinkgreve et al. (2018) is $3E_{50}^{\text{ref}}$.

3 Validation of numerical modelling method

The results of the micro-tunnel model based on the geotechnical conditions of the North/South Metro Line Amsterdam cannot be validated by field data. To confirm the reliability of modelling method, a 3D model was established based on the centrifuge model test conducted by Loganathan et al. (2000) and following numerical simulation by Lee and Ng (2005). The same soil profile, pile parameters, and location of pile relative to the axis of the tunnel from the centrifuge test were adopted to provide a basis for comparison. After validation of the prior model, it was adjusted to fit the case of micro-tunnelling but modelling technique and design methods were kept in the same.

3.1 Model Geometry

As shown in Figure 6. A 6m diameter circular tunnel was excavated in the stiff homogenous over-consolidated deposit of London clay with a cover depth of 15m. A 0.8 m diameter pile by the length of 18m was located 5.5 m from the tunnel horizontal axis. All parameters were kept in the same with those from the centrifuge test.

Contrasted to the centrifuge test conducted in plane strain condition, the numerical model in PLAXIS was built in three-dimensional condition to get more accurate simulation and be prepared for the later micro-tunnel models. The longitudinal sketch of the model is shown in Figure 7. The TBM shield with conical shape was simulated and behind it, there was an unsupported span with the length of $0.25D$, which modelled the grouting phase during excavation. D is the diameter of the TBM shield. The final lining sections were erected after the grouting phase. The excavation started from $1D$ ahead of the plane where pile located and stopped $2.5D$ away from the pile. Pile responses were taken from the last stage and compared with results from the centrifuge test.

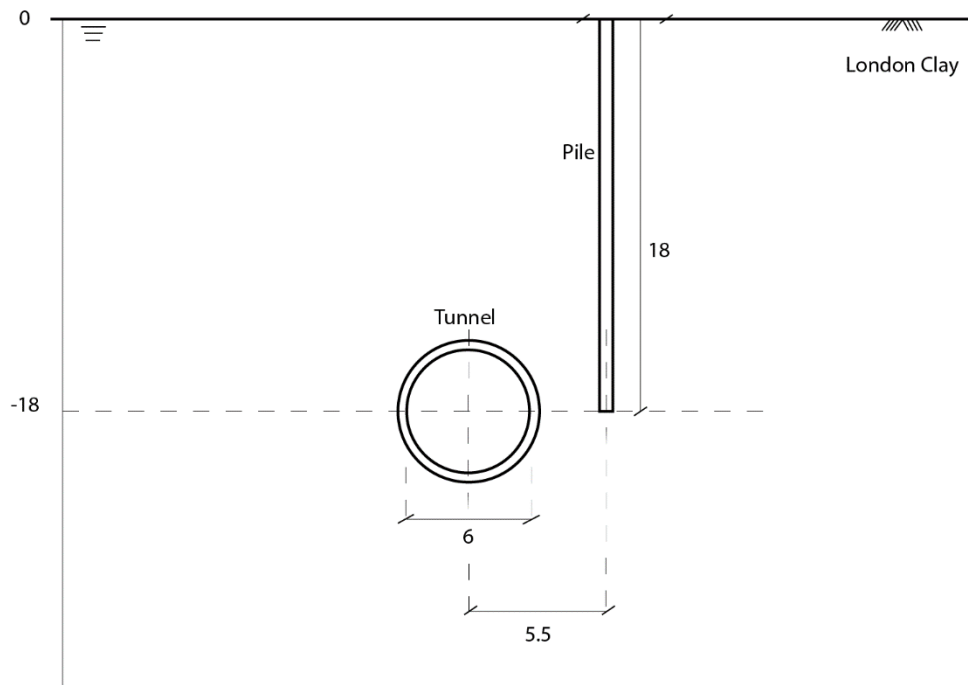


Figure 6. Configuration of the London Clay model

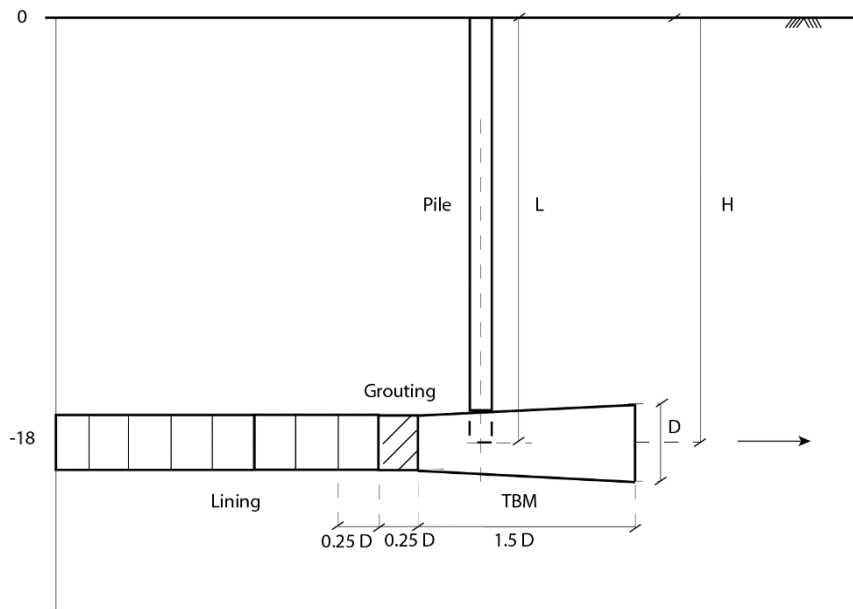


Figure 7. Sketch of London Clay model in the longitudinal direction

3.2 Constitutive Model and Model Parameters

Following the set-up of numerical simulation conducted by Lee and Ng (2005), the Mohr-Coulomb model was adopted for London clay. Parameters of soil are illustrated in Table 2. Properties of TBM are summarized in Table 3. The tunnel shield, final lining and concrete pile were modelled as linear elastic materials. Properties were kept the same with those used in the centrifuge test (Loganathan et al., 2000) and were listed in Table 4 below.

Table 2. Properties of The Mohr-Coulomb model used in the London Clay model

	Value	Unit
Unsaturated bulk unit weight γ_{unsat}	18	[kN/m ³]
Saturated bulk unit weight γ_{sat}	20	[kN/m ³]
Vertical effective Young's modulus E'_v	7500 + 3900z*	[kN/m ²]
Angle of dilation ψ	11	[°]
Effective angle of friction ϕ'	22	[°]
Effective cohesion c'	5	[kN/m ²]
Undrained shear strength c_u	75	[kPa]
Coefficient of permeability k	1×10^{-9}	[m/s]

Table 3. Properties of the tunnel bored machine in London Clay model

	Value	Unit
Horizontal axis depth (H)	15	[m]
Diameter of tunnel (D)	6	[m]
Length of TBM (L_{TBM})	9	[m]
Length of grouting section	1.5	[m]
Length of single lining	1.5	[m]
Length of pile (L)	18	[m]
Diameter of pile (d)	0.8	[m]
Working load of pile (F)	1313	[kN]

Table 4. Properties of concrete, shield and pile

	Value			Unit
	Concrete	TBM shield	Pile	
Young's modulus E	3.1×10^7	2×10^8	2.785×10^7	[kN/m ²]
Bulk unit weight γ	27	247	24	[kN/m ³]
Poisson's ratio	0.1	0	-	[-]

3.3 Mesh generation

A plane of symmetry was identified at the vertical axis of the tunnel and only half of the domain was modelled. As shown in Figure 8, the mesh was 80m long, 60m wide, 36m high at prototype scale, consisting of 30118 soil elements and 44907 nodes. The main consideration of the size of the model is to make all influenced elements included in the mesh. Most of the soil clusters took coarseness factor as 1 but clusters around the tunnel and pile were refined and the factor was set to 0.5.

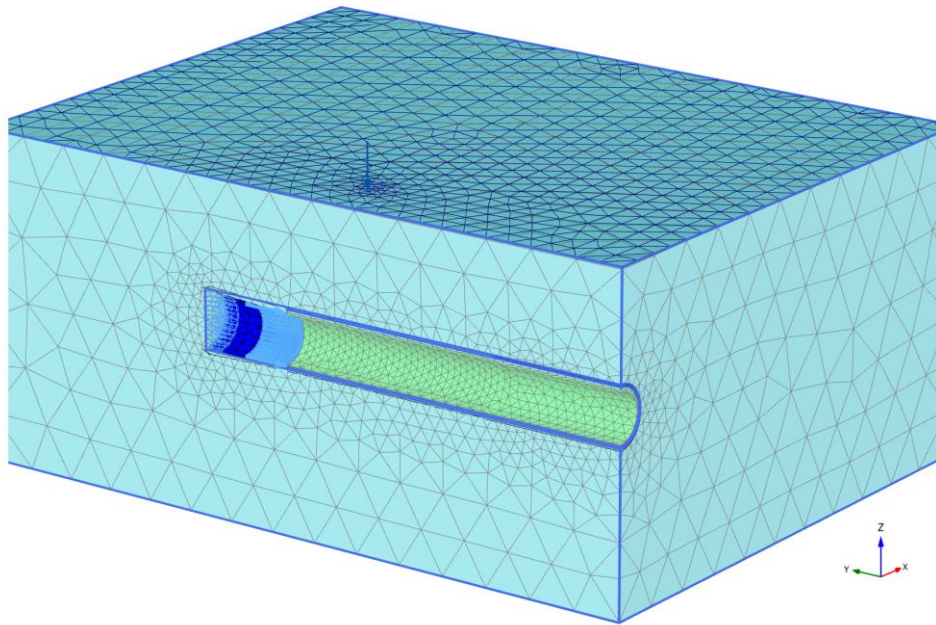


Figure 8. Mesh of the model in PLAXIS 3D

3.4 Numerical modelling procedures

Simulation of TBM excavation process mainly followed PLAXIS 3D (Brinkgreve et al., 2013). There are several features in PLAXIS 3D when the phased excavation of a shield tunnel is simulated. First, the conical shape of the shield of TBM was simulated by pre-described surface contraction. Second, the unsupported span behind the machine can model the grouting phase. Main steps are summarized as follows and more details of modelling will be introduced in models of micro-tunnelling:

1. Generation of the initial stresses using the K_0 procedure.
2. Activating the pile and working load.
3. Full dissipation of excess pore pressures developed in response to the applied load. Initializing the displacement to zero.
4. Excavation of tunnel. The excavation started from 1D ahead of the pile. Volume loss was set to be 1% to make it identical with the condition of the centrifuge test.

5. TBM advanced till the tunnel face was $2.5D$ beyond the pile transverse section. The final position of the TBM is illustrated in Figure 9.
6. Pile responses were obtained after the tunnel reached the final position when the pile was at a plane strain condition.

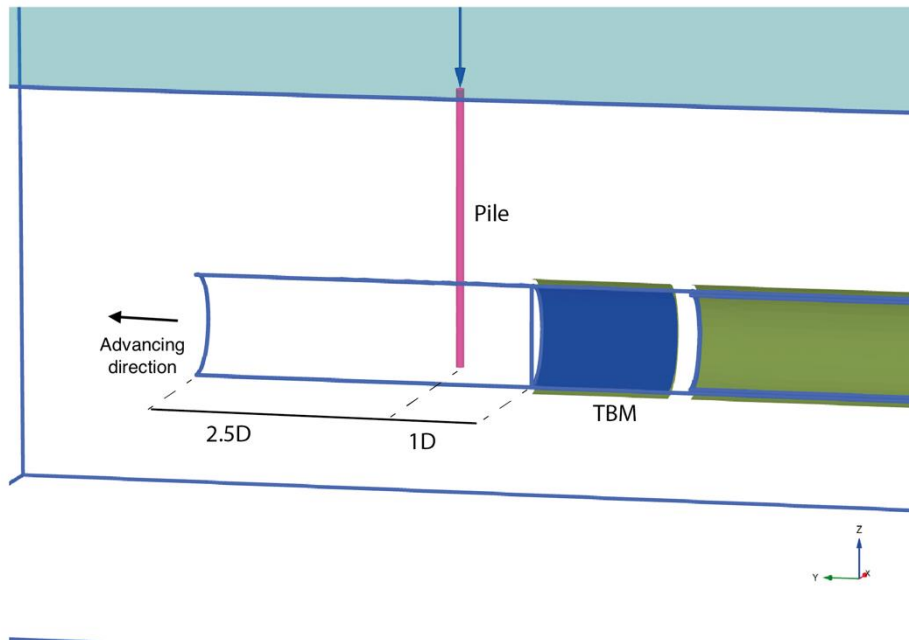


Figure 9. Sketch of the advancement of the TBM

3.5 Comparison of results between the centrifuge test and the numerical model

The reliability of the model was evaluated by comparing the results of the numerical model with those measured data from the centrifuge test. The comparison includes 4 aspects, which are surface settlement, lateral soil movement, pile later movement and pile head movement.

3.5.1 Surface settlement

The comparison of surface settlement induced by tunnelling is illustrated in Figure 10. Results of numerical modelling were exactly same with the measured settlement from centrifuge test, indicating that the soil constitutive model used in modelling can represent the soil behaviour well and the numerical simulation of tunnel excavation part was reliable.

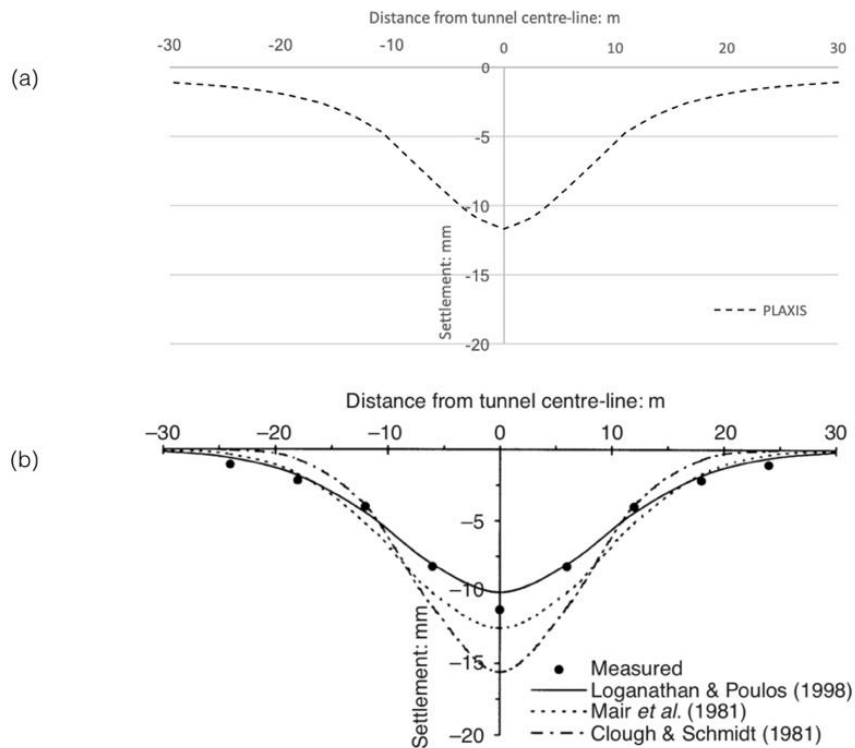


Figure 10. Surface settlement trough (a) numerical prediction in PLAXIS (b) measured and analytical results from Loganathan et al. (2000)

3.5.2 Soil lateral movement & Pile lateral movement

Results of soil lateral movements from numerical simulation and centrifuge test are demonstrated in Figure 11. Soil lateral movement in the numerical model was the same as that in the centrifuge test and the maximum value happened at the horizontal axis of the tunnel.

Figure 12 shows the pile lateral responses due to tunnelling. For numerical simulation, the pile deformed in the same trend and only small difference was observed at the pile tip, where the lateral movement of the pile in numerical simulation was 6.4mm while the value in the centrifuge test was 7.2mm. One scenario to explain this is about the embedded beam model used to simulate pile. In PLAIXS, an embedded beam is used to simulate pile, but it is not a real volume element. A zone in the soil volume surrounding the beam is identified where any kind of soil plasticity is excluded to make the embedded beam almost behave like a volume element. At corners of this zone, high peaks in stresses and strains might occur and stiffness of clusters representing the beam could increase. This problem can be relieved by refining the coarseness factor of clusters near the embedded beam.

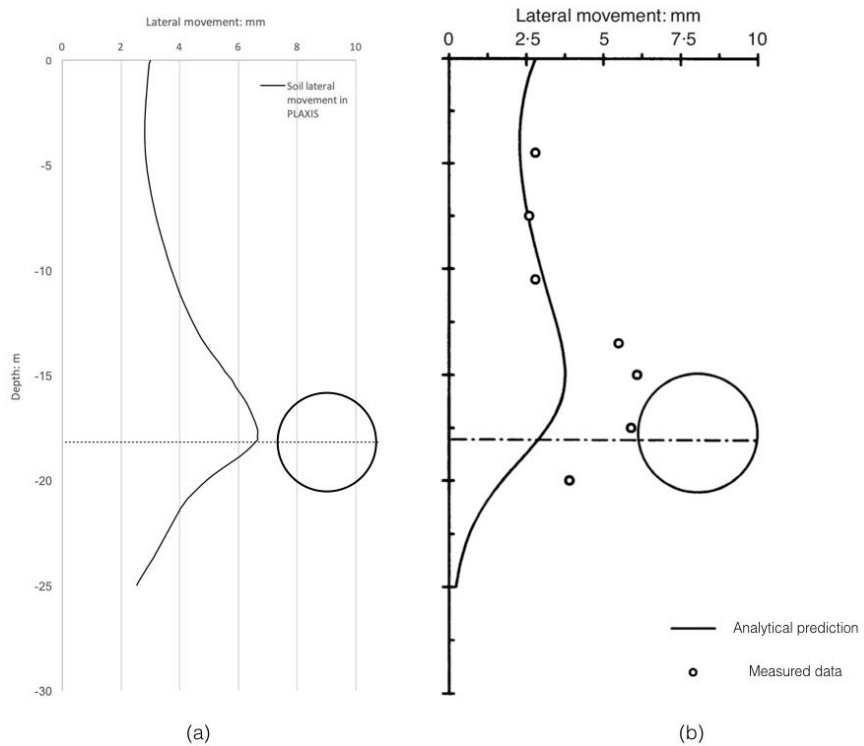


Figure 11. Soil lateral movement (a) numerical prediction in PLAXIS (b) measured and analytical results from Loganathan et al. (2000)

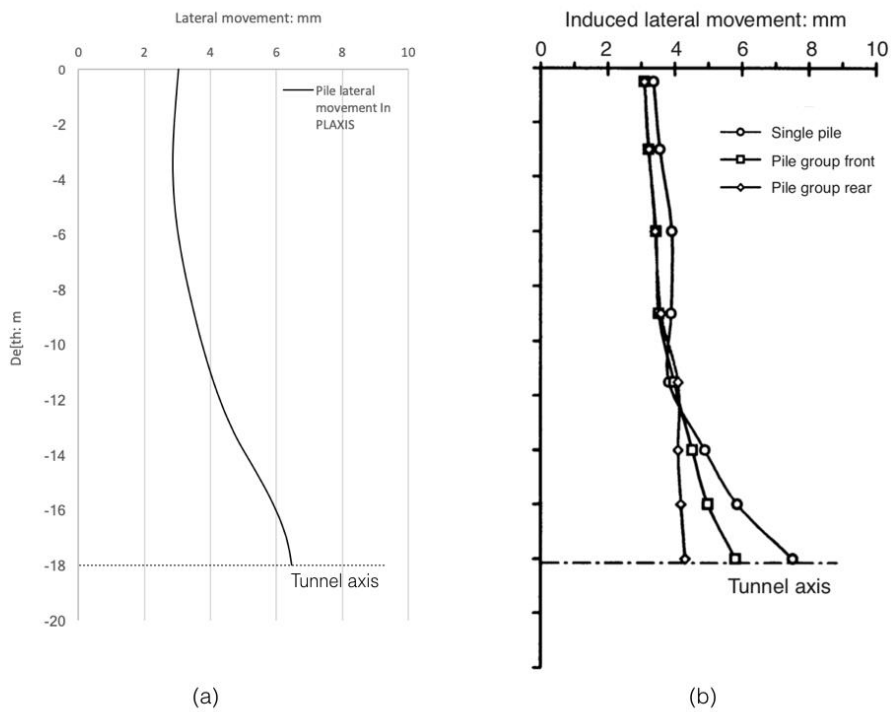


Figure 12. Pile lateral movement (a) numerical prediction in PLAXIS (b) measured and analytical results from Loganathan et al. (2000)

3.5.3 Pile head settlement & relative settlement at the tip

Pile head settlement and lateral deflection were recorded and compared with those in the centrifuge test, as shown in Table 5. Although the values showed good agreement, it barely demonstrates the load transfer mechanism of the pile due to the tunnelling process. Because of this, Table 5 gives the relative settlement at pile tip and Table 6 shows the change of base load, which were not mentioned in the centrifuge test. For better comparison, the pile load exerted on the pile head was 1340kN, which was the same with that in the centrifuge test. Based on these two parameters, it is believed that the shaft capacity of the pile decreased because of the excavation and the pile base had to support a larger part of the load. Besides, the small amount of relative pile head settlement indicates that the shaft capacity was going to be fully mobilized and after that, an abrupt increase of relative settlement can be observed.

Table 5. Pile head settlement, lateral deflection and relative settlement

	Pile head settlement	Lateral deflection	Pile head relative settlement	Unit
Numerical simulation	11.03	3	4.02	[mm]
Centrifuge test	11.8	4.4	-	[mm]

Table 6. Change of base load due to tunnelling

	Base load [kN]
Before tunnel excavation	60.3
After tunnel excavation	276

3.6 Conclusions regarding the reliability of the numerical modelling method

Based on the comparison of results from numerical modelling and centrifuge test, it is believed the numerical modelling methods used in PLAIXS 3D are capable to predict the soil and pile responses due to tunnelling. Besides, there are several things should be mentioned and noticed in later models.

1. The soil constitutive model used in the case of London Clay is the Mohr-Columb Model which has been proven to be capable to give a good simulation of soil behave. However, no pile failure happened in the model means that the plasticity characteristics of the soil model were not tested. Considering the next two models may include pile failure under large volume loss, a more advanced model concerning plastic performance, The Harden Soil model, was adopted for later models.
2. Compared with analytical predictions illustrated in Figure 10 and Figure 11, the numerical model gave a batter prediction of soil movements and pile settlements. However, the accuracy of prediction for the pile lateral movement was not as good as others. The pile lateral movement was little smaller than the measured value.

4 Details of the numerical modelling procedure

After validation of the numerical modelling method, it was used to model the case of micro-tunnel. Some modifications were made to transform the method into the one for the micro-tunnelling situation. Details of the model of micro-tunnel and description of the modelling procedure are introduced in this chapter.

4.1 Ground conditions and soil profile

The model simulates the characteristic geology of the centre of Amsterdam described by Delfgaauw et al. (2009). The model extends to -40m. As shown in Figure 13, at the bottom, there is a fluvio-glacial medium sand layer (S2) depositing in the Saalian period. Above this glacial deposit, marine clays of Eemian age (C1) is the stratum where the micro-tunnel is excavated. This clay layer is overlain by two medium to dense aeolian (first) and fluvial (second) sand layers which are combined into one layer in the model (S1). The upper layers, the Holocene deposits (D) including tidal sand and mainly of soft clay and peat layers, have also been condensed into one layer.

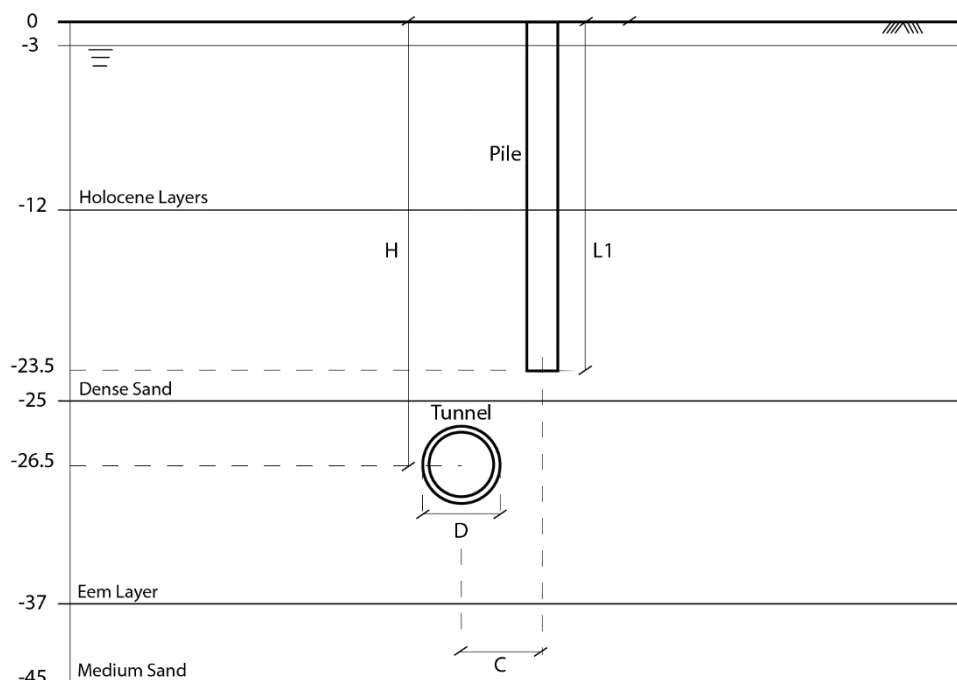


Figure 13. Sketch of soil profile based on the description of Delfgaauw et al. (2009)

4.2 Material constitutive models

All layers are modelled with the Harden Soil (HS) model. Table 7 gives an overview of the soil layers and their properties and parameters. Dilatancy is not considered in this model. The drainage types are all drained except the clay layer. The permeability of the clay layer is 2×10^{-9} m/s in all directions. The power in the strength-dependency stiffness relationship is 0.5 for all layers. Interface stiffnesses for soils were 0.63 except the Clay layer, which was 0.7. The hydrostatic pore pressure distribution in the model is derived from a phreatic level at 3 m below the ground level.

Table 7. Four soil layers and their properties in the model of MTBM

	Top (NAP) [m]	γ_{unsat} [kN/m ³]	γ_{sat} [kN /m ³]	E_{50}^{ref} [kN /m ²]	$E_{\text{ode}}^{\text{ref}}$ [kN /m ²]	$E_{\text{ur}}^{\text{ref}}$ [kN /m ²]	ϕ' [°]	c' [kN /m ²]	OCR [-]
D	0	13	15	8000	8000	24000	28	3	n/a
S1	-12	17	19	34000	34000	102000	34	0	n/a
C	-25	16	18	11000	11000	33000	32	15	2
S2	-37	17	19.5	25000	25000	75000	33	0	n/a

4.3 Micro-tunnelling parameters for analysis

4.3.1 Properties of micro-tunnel boring machine

The micro-tunnel boring machine (MTBM) is modelled based on AVN1600AB (standard) machine from company Herrenknecht. Table 8 gives technical data of the machine. The shield of MTBM and concrete material used as lining were linear elastic materials and details are listed in Table 9.

Behind the MTBM, there was an unsupported span with the length of 3D to simulate the lubrication phase during the excavation process. After that, the final lining was modelled with a length of 0.75D for each section. The sketch of the whole model in the longitudinal section is shown as Figure 14, where L1 is the length of pile, H is the axis depth of MTBM, D is the outer diameter of MTBM and S is the distance between the bore front and the plane where the pile located. Specific values are listed in Table 10.

Table 8. MTBM properties

	Value	Unit
Horizontal axis depth H	-26.5	[m]
Outer diameter of shield	1970	[mm]
Outer diameter of pipe	1940	[mm]
Inner diameter of pipe	1600	[mm]
Maximum single weight	22000	[kg]
Length of Shield	7	[m]

Table 9. Properties of MTBM shield and lining

	MTBM shield	Final lining	Unit
Thickness* d	0.1	0.17	[m]
Type of behaviour	Elastic; isotropic	Linear elastic	[-]
Unit weight above phreatic level γ_{unsat}	247	27	[kN/m ³]
Young's modulus E	2×10^8	3.1×10^7	[kN/m ²]
Poisson's ratio ν	0	0.2	[-]

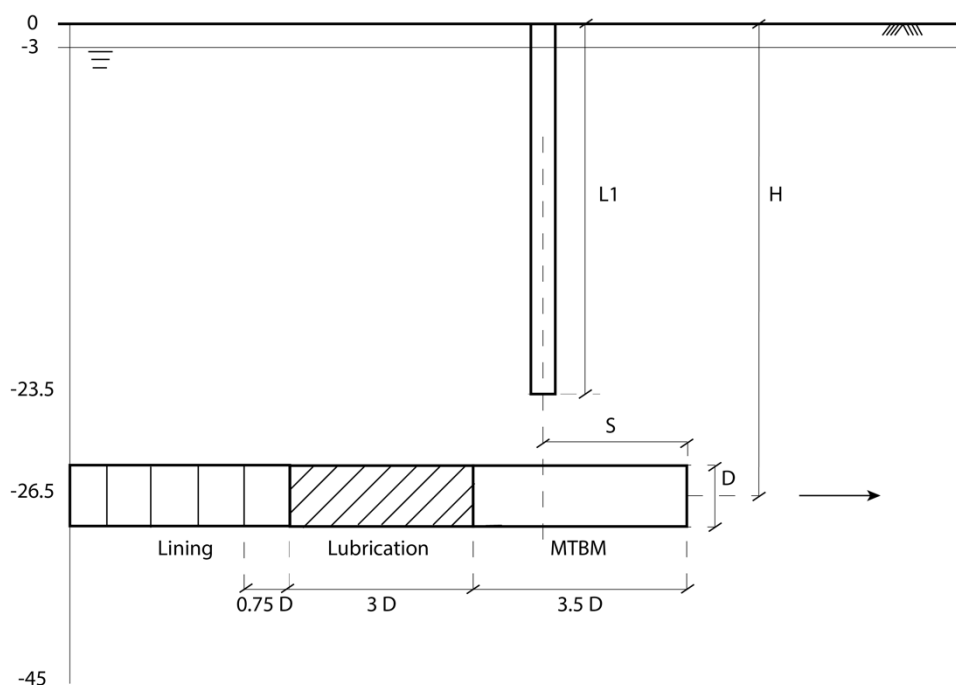


Figure 14. Sketch of MTBM in the longitudinal direction

Table 10. Length of sections of MTBM model

	Absolute Value [m]	Relative Value
Length of MTBM Shield	7	3.5D
Length of Lubrication part	6	3D
Length of single lining	1.5	0.75D

4.3.2 The shape of the MTBM shield

In PLAXIS 3D, a prescribed contraction is added to the shield of TBM considering the conical shape of the shield. It is the main source of soil convergence during the modelling of TBM. For the case of MTBM, the shape of the shield is columned, and the contraction is not activated because it was assumed the volume loss occurred mainly at lubrication phase. Therefore, in this PLAXIS 3D model, the micro-tunnel machine was simulated as a 7m long column with even diameter of 1.97m.

4.3.3 Tunnel face stability

In PLAXIS, the default type of tunnel boring machine is Earth Pressure Balance shield, as an implicit assumption. The tunnel face pressure consists of two parts, which are the ground and water pressure on the head and the penetration resistance of the boring wheel. To maintain the bore front stability, the front pressure should be controlled between a minimum and a maximum front pressure. In PLAXIS 3D, the front pressure is set to be perpendicular to the cutting face and increasing linearly with depth.

4.3.3.1 Minimum front pressure

The minimum front pressure is derived from active stability of the bore front which prevents the soil collapse into the bore shield. The pressure at the crown $\sigma'_{h,tot,ref,min}$ is given by Equation 1:

$$\sigma'_{h,tot,ref,min} = \gamma' \times K_a \times h_{crown} + \gamma_w \times h_{crown} + I_r \quad 1$$

$$\Delta\sigma'_{h,soil,inc,min} = \gamma' \times K_a + \gamma_w \quad 2$$

$$K_a = \frac{1 - \sin \phi'}{1 + \sin \phi'} \quad 3$$

where γ' is effective soil unit weight; h_{crown} is the depth at the crown of micro-tunnel; $\Delta\sigma'_{h,soil,inc,min}$ in Equation 2 is the incremental earth pressure; K_a is active earth pressure coefficient; ϕ' is the effective angle of internal friction of soil. I_r , the penetration resistance of the boring wheel is the force to cut open the ground. An assumption is made that I_r is evenly distributed at the cutting face and equal to 50kN/m² according to NE3650.

4.3.3.2 Maximum front pressure

The maximum front pressure $\sigma'_{h,tot,ref,max}$ is determined by the principle of passive stability of the bore front that avoids the soil being pushed away from the bore front as shown in Equation 4:

$$\sigma'_{h,tot,ref,max} = \gamma' \times K_p \times h_{crown} + \gamma_w \times h_{crown} + I_r \quad 4$$

$$\Delta\sigma'_{h,soil,inc,max} = \gamma' \times K_p + \gamma_w \quad 5$$

$$K_p = \frac{1 + \sin \phi'}{1 - \sin \phi'} \quad 6$$

where the K_p is the passive earth pressure coefficient.

During the modelling process, the front pressure was adjusted for several times till no obvious horizontal movement of soil occurred at the front face. As a result, 1.3 times of active earth pressure was adopted for the specific geotechnical condition.

4.3.4 Overburden pressure of soil

There are two assumptions for soil pressure caused by overburden. Firstly, the soil stresses are equal to the undisturbed situation before installation of the tunnel. The second assumption is that the soil pressure is perpendicular to the lubrication surface and increasing linearly with depth, which is given by:

$$\sigma'_{\text{ref}} = u + \gamma' \cdot h_{\text{cen}} \quad 7$$

$$\sigma'_{\text{inc}} = u + K_0 \cdot \gamma' \cdot h_{\text{cen}} \quad 8$$

$$K_0 = 1 - \sin \phi' \quad 9$$

where σ'_{ref} in Equation 7 is soil pressure at the centerline of micro-tunnel; σ'_{inc} in Equation 8 is the incremental soil; u is pore water pressure at the centerline; h_{cen} is the depth at the centerline of micro-tunnel; K_0 is neutral earth pressure coefficient.

4.3.5 Lubrication and soil convergence

To decrease the friction between pipe and soil, lubrication exists for the whole length of MTBM. In PLAXIS 3D, the relative movement of MTBM and soil cannot be simulated directly so the induced friction is not introduced in this case. Behind the shield of MTBM, a lubrication phase with the length of $6D$ was created and evenly distributed lubrication pressure q_L is exerted to the surface. The lubrication pressure is set to be smaller than overburden pressure, so the convergence of soil occurred in this part. Refer to different lubrication pressure, there were different volume loss ratios and so did piles response.

4.3.6 Volume loss

Contraction mainly occurs at lubrication phase due to the difference between lubrication pressure and soil pressure. The pressure ratio r between lubrication pressure q_L and soil pressure q_O is calculated as Equation 10:

$$r = \frac{q_L}{q_O} \times 100\% \quad 10$$

Because the adjacent soil was compressed by the installation of the pile before micro-tunnel excavation. For different lubrication pressure, the tunnel can contrast to a different extent. It should be mentioned that for different configurations of pile and micro-tunnel, the same lubrication pressure could lead to different volume loss ratio ε .

$$\varepsilon = \frac{OD_{\text{shield}}^2 - OD_{\text{pipe}}^2}{OD_{\text{shield}}^2} \times 100 \quad 11$$

Table 11 shows the relationship between pressure ratio and induced volume loss for the case of the deep tunnelling model built in PLAXIS 3D. In that model, the volume loss ratio was 3% to simulate the realistic excavation process.

Table 11. Relationship between pressure ratio and volume loss

Pressure ratio r	Volume loss ratio ε
100,0	0,3
89,9	0,6
84,8	0,7
79,9	0,8
70,0	1,2
60,0	1,7
50,1	2,5
47,8	2,9
46,0	3,3

4.3.7 Lining

After the stress relaxation, the final lining is activated, and the thrust force is exerted to the lining cross section. The thrust force is estimated with the empirical formula of Krause (1987).

$$p_v = \beta \cdot D^2 \quad 12$$

where p_v is thrust force; β is an empirical factor which is between 500 and 1200. In this model, the maximum value 1200 is chosen for safety; D is the diameter of micro-tunnel.

4.3.8 Summary of properties

Based on theoretical and empirical methods mentioned above, a model of micro-tunnel was built in PLAXIS 3D. Table 12 lists all properties of the MTBM used in the model.

Table 12. Properties of MTBM model created in PLAXIS 3D

	Notation	Value	Unit
Diameter of the shield	D	1.97	[m]
Face pressure	$\sigma'_{h,tot,ref}$	446.1	[kN/m ²]
	z_{ref}	25.5	[m]
Thrust force	$\Delta\sigma'_{h,soil,inc}$	18	[kN/m ²]
	p_v	4657	[kN]
Pressure ratio	r	42.1	[%]
Volume loss ratio	ε	3	[%]

4.4 Pile parameters for analysis

4.4.1 Properties of the bored concrete pile

The parameters of the concrete pile used in models are listed below in Table 13:

Table 13. Properties of the bored pile used in the MTBM model

	Concrete pile	Unit
Diameter	0.8	[m]
Type of behaviour	Linear elastic	[-]
Unit weight γ	24	[kN/m ³]
Young's modulus E	3.5×10^7	[kN/m ²]
Poisson's ratio ν	0.1	[-]
Spacing* L	5	[m]

4.4.2 Shaft resistance of pile

Piles in this project were modelled by embedded beams in PLAXIS to simulate the interaction of them with the surrounding soil. A data set for embedded beam representing pile can be found in PLAXIS and in these parameters, shaft resistance and base resistance of pile are critical to model the behaviour of pile correctly.

For the shaft capacity, it can be inputted by Linear option or Layer dependent option. The former option needs the user to define the skin resistance at the beginning and the end of the embedded beam so that the shaft capacity F_{skin} can be generated by Equation 13:

$$F_{skin} = \frac{1}{2} L_{pile} (T_{skin,start} + T_{skin,end}) \quad 13$$

where L_{pile} is the pile length. $T_{skin,start}$ and $T_{skin,end}$, as two inputs, are measured skin resistance at the top and bottom of the pile, respectively.

The latter one, Layer dependent option is used to relate the shaft resistance to the strength properties and the interface strength reduction factor of surrounding soils:

$$T_{skin} = c_i + \sigma'_n \tan \varphi_i \quad 14$$

$$c_i = R_{inter} c_{soil} \quad 15$$

$$\sigma'_n = K_0 \sigma'_v \quad 16$$

$$\tan \varphi_i = R_{inter} \tan \varphi_{soil} \quad 17$$

where T_{skin} is the local skin resistance of the interface. c_i and φ_i are the cohesion and the friction angle of the interface, respectively. They are connected with corresponding soil properties c_{soil} and φ_{soil} by interface strength reduction factor R_{inter} . σ'_n is the horizontal effective stress of the soil. K_0 is the coefficient of lateral earth pressure and σ'_v is the vertical effective stress of the soil.

Since the in situ data of piles were lacked in this project but the soil properties were provided. The latter option, Layer dependent option was chosen for the skin resistance of piles.

4.4.3 Base resistance of pile

The bearing capacity for compression piles is generally performed using the 4D/8D Koppejan method, which is a CPT based method for pile calculations. Since the lack of CPT data, the bearing capacity was calculated from base resistance and skin resistance separately. Base resistance F_{base} is given by APIRP2A (2006):

$$F_{base} = \pi R^2 N_q \sigma'_v \quad 18$$

where R is the radius of the pile. N_q is a dimensionless bearing capacity factor dependent on the soil internal friction angle, which is variable due to different sand density. For medium sand, the factor could be 20 to 40 and for dense sand, it could be up to 50. Considering the dense sand layer where the pile tip was located and several tests conducted for the pile behavior, it was selected to be 33 at the beginning in this project.

Here are some examples of pile bearing capacity inputted in models.

Table 14. Beading capacities of piles with different lengths

Length [m]	Diameter [m]	Shaft resistance [kN]	Base resistance [kN]	Bearing capacity [kN]
20.5	0.8	611.7	2662.3	3274
22.5	0.8	710.6	2960.8	3671.4
23.5	0.8	760	3110	3870

4.5 Mesh generation

A plane of symmetry was identified at the vertical axis of the micro-tunnel and only half of the domain was modelled. The dimensions of the model were determined via the dimension rules (Equation 19&20) given by COB-L520 (1999), which are based on the overburden height (H) and the diameter of the tunnel (D). The rules ensure that all soil clusters impacted by the tunnelling were included in the model. Based on these rules, the mesh was 90m long, 50m wide and 45m high at prototype scale.

$$\text{Width of model} \geq 1.5 \times (H + D) = 41.25 \text{ m} \quad 19$$

$$\text{Height of model} \geq H + 2D = 29.5 \text{ m} \quad 20$$

Most of the soil clusters took coarseness factor as 0.125 but clusters around the micro-tunnel and the pile were refined and the factor was set to 0.0625.

4.6 Modelling of phased excavation

Compared with the way to model the phased excavation of a shield tunnel, the method of micro-tunnel has some differences. First, the conical shape of the machine was not simulated considering the relatively small size of MTBM. Second, the unsupported span behind the MTBM was extended to the length of 3D to simulate the lubrication phase in the micro-tunnel excavation process. Third, the lubrication pressure was set to be smaller than the overburden pressure so that the contraction occurred at the lubrication phase which was the main source of the volume loss. The excavation procedure comprised steps:

1. The initial phase

The initial phase concerns the generation of the initial stresses using the K_0 procedure. The default settings in PLAXIS 3D are adopted for the initial phase.

2. Installation of pile

A bored pile was introduced in greenfield firstly. In PLAXIS 3D, the installation procedure of pile and induced surrounding soil movement cannot be modelled perfectly. For the reason of simplification, the case of the bored pile was first considered. The default method to model the bored pile in PLAXIS 3D is valid, in which the soil cluster is deactivated and then the embedded beam is activated. Although the compression of adjacent soil due to the installation of the pile is ignored in this method, it is still acceptable considering the relatively small disturbance of bored pile in reality. After the pile activated, the vertical working load was added to the pile head throughout of the excavation.

3. The initial position of micro-tunnel boring machine

Allowed full dissipation of excess pore pressures developed in response to the applied load. In this first phase, it was assumed that the MTBM has advanced 10m and the machine was only placed at

the initial position rather than moving forward. The displacement caused by the last phase was set to zero because only the settlement induced by tunnelling is the interest of this research. After that, the tunnel was introduced, and the enclosed soil cluster was switched off.

4. Advancement of MTBM

Advancement of micro-tunnel was finished in several steps. The MTBM started from 10m ahead of the pile and advances in $0.5D$ rounds. Behind the MTBM, there was an unsupported span with the length of $3D$ to simulate the lubrication phase during the excavation process. Contraction mainly occurred in this part. After that, the concrete linings with the length of $0.75D$ were applied to support the surface of the micro-tunnel. The excavation was repeated until the tunnel stopped at 10m behind the pile. When the micro-tunnel arrived the final position, the area where the pile was located was approaching plane strain condition. The responses of the pile due to tunnelling were collected in the final phase.

5 Models simulated in PLAXIS 3D

Two 3D models representing shallow tunnel condition and deep tunnel condition, respectively, were firstly built in PLAXIS 3D. Different pile deformation mechanisms were figured out and will be elaborated below. Before these, a working load test was firstly conducted in PLAXIS 3D to calibrate the behaviour of the bore pile.

5.1 Pile load test

Before modelling the excavation of micro-tunnel, it is important to get a comprehensive study of pile behaviours under working load in a specific geotechnical condition. Besides, in PLAXIS, bearing capacity of the pile is an input value rather than the result of finite element calculation. Due to this reason, the calibration of the pile is necessary.

A numerical pile load test was executed in PLAXIS 3D based on the same geotechnical condition of Amsterdam. Figure 15 shows the relationship between exerted load and pile head settlement of the pile with a length of 23.5m. For the pile with the specific length of 23.5m, the ultimate bearing load is 3870kN and the ultimate settlement is 168.7mm, which is 21.1% of the diameter. Based on criteria of bored piles from NEN9997-1+C2 (2017), the extreme settlement of bored pile at failure state should be 20% of the diameter. Figure 16 illustrates the pile settlements in the way of NEN9997-1+C2 (2017). It is believed that the model of the bored pile can provide reliable responses in later experiments.

After the ultimate bearing load had been determined, the working load for the pile with a Factor of Safety of 3 was calculated as 1135kN and was applied to the pile head throughout the experiment. An initial settlement occurred due to the working load as recorded in Table 15. Considering the goal of experiments is to investigate the pile responses because of tunnel excavation. The initial settlement was not included, and the ground settlement was set to be zero before excavation.

The working load test was conducted for every pile length and the table shows results of all piles used in 3D condition.

Table 15. Initial settlements of piles with different lengths

Diameter [m]	Length [m]	Bearing capacity [kN]	Working load [kN]	Initial settlement [mm]
0.8	20.5	3270	1090	16.7
0.8	21.5	3470	1160	15.7
0.8	22.5	3670	1225	14.9
0.8	23.5	3870	1135	12.8

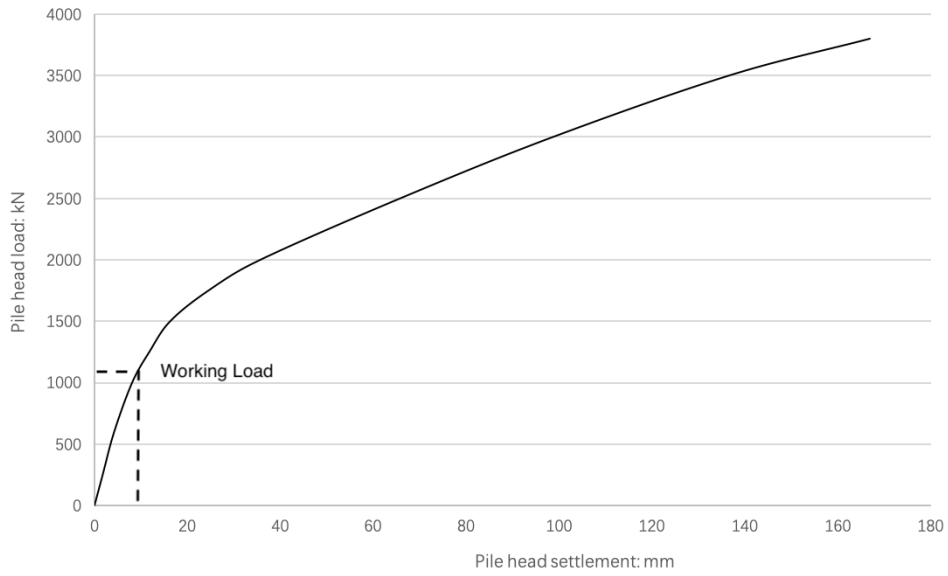


Figure 15. Pile head settlement with different pile head loads

Table 16. Pile head settlements with the increasing working load

Load (kN)	Pile head settlement (mm)
0	1,8
250	3,56
600	6,04
1000	9,9
1250	13,6
1500	18,1
1750	26,34
2000	37,5
2500	67,6
3000	100,5
3500	138,4
3870	168,7

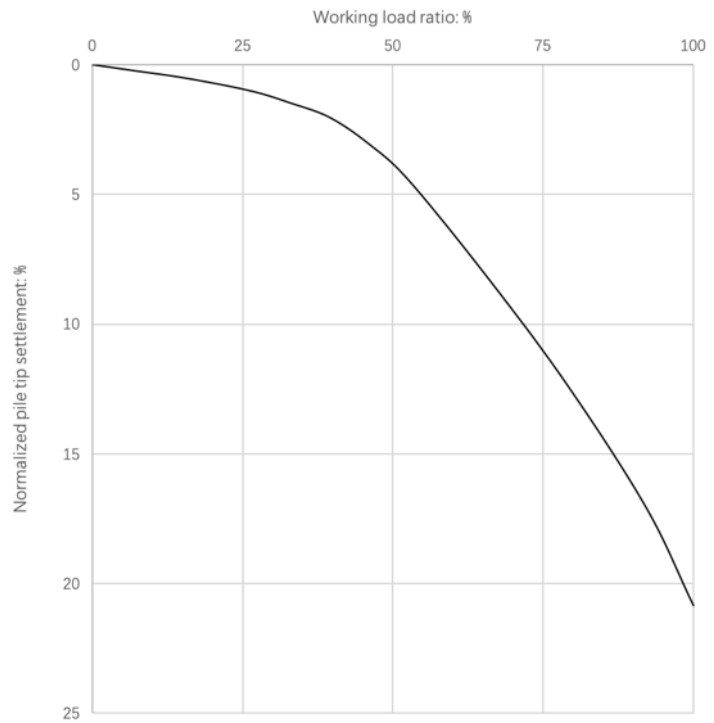


Figure 16. Pile head settlement curve in the form of NEN9997-1+C2 (2017)

5.2 Deep tunnel condition

5.2.1 Geometry

In the deep tunnelling model, the MTBM is 3m below the 23.5m pile as shown in Figure 17. Other parameters of the configuration are listed in Table 17.

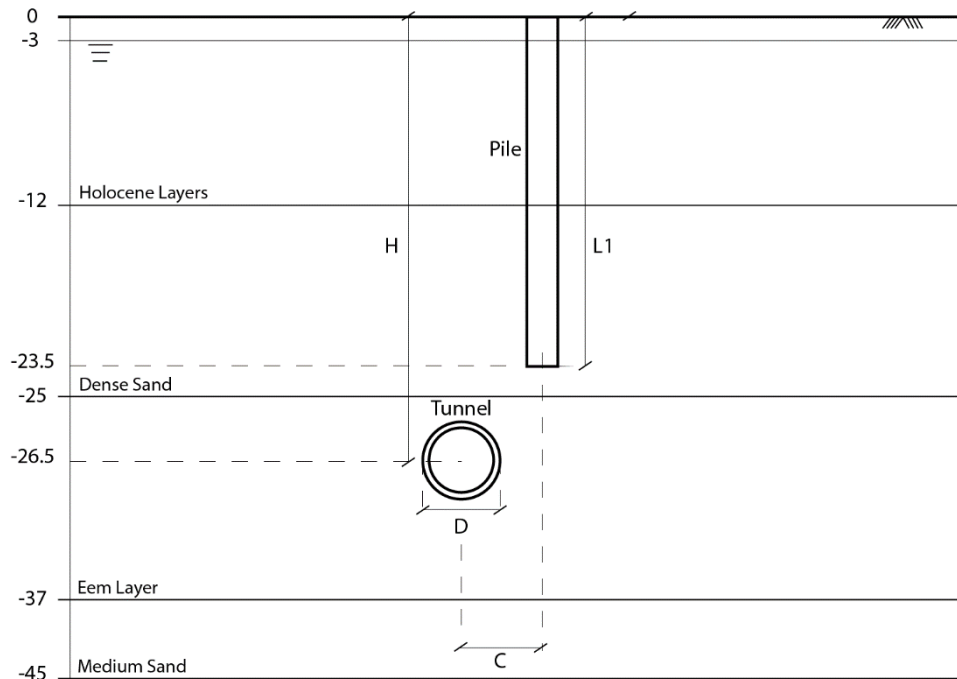


Figure 17. Sketch of the deep tunnel model

Table 17. Parameters of the configuration of the deep tunnel model

	Notation	Value [m]
Pile length	L1	23.5
Tunnel diameter	D	1.97
Embedded depth at the axis of the tunnel	H	26.5
Horizontal Clearance	C	1

5.2.2 MTBM advancement

The identical advancement process of MTBM in the longitudinal direction was simulated in both two conditions. It should be mentioned that in MTBM models, the distance between the bore front of the machine and the plane where the pile located was taken to describe the advancement of MTBM, as shown in Figure 18. In both shallow tunnelling and deep tunnelling conditions, the machine started from $-4.5D$, namely 9m behind the pile and stopped at $17.5D$, which is 35m ahead of the pile.

In two models, the volume loss ratio ε was both set to 3%, which represents the real situation concerning the specific MTBM machine, assuming the gap between the shield and pipe was fully closed.

$$\varepsilon = \frac{OD_{shield}^2 - OD_{pipe}^2}{OD_{shield}^2} \times 100\% = \frac{1970^2 - 1940^2}{1970^2} \times 100\% = 3\% \quad 21$$

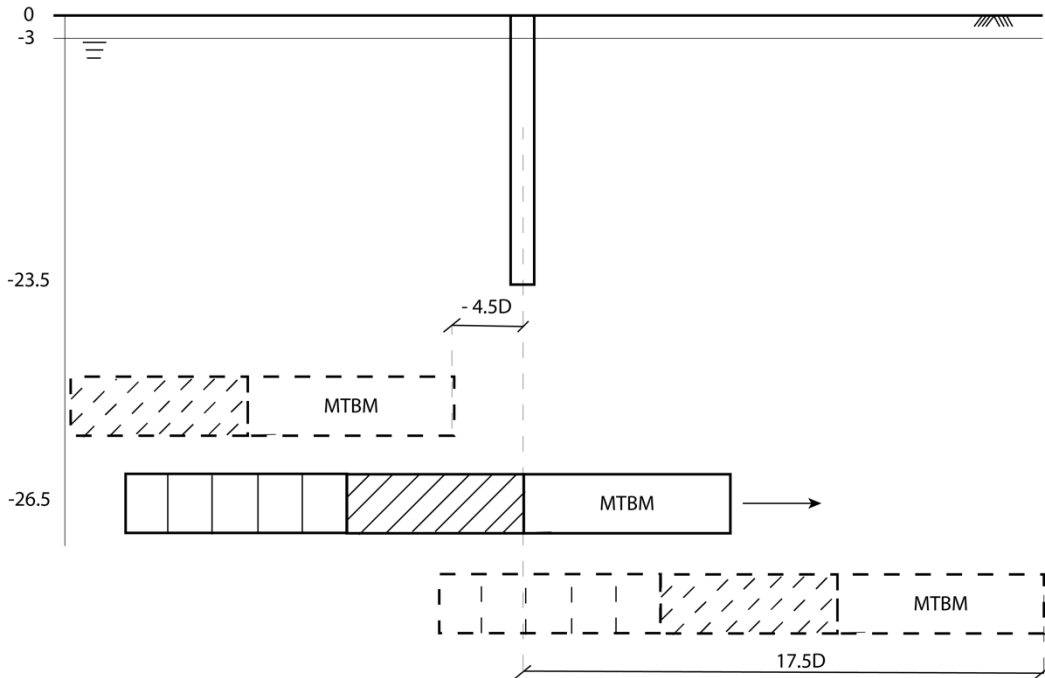


Figure 18. Sketch of the advancement of the MTBM model

5.2.3 Pile responses induced by tunnelling

Pile responses are divided into two parts, which are the load transfer mechanism and pile movement due to tunnelling.

5.3.2..1 Load transfer mechanism

The changes of axial load and shaft friction of the pile were illustrated in Figure 19 and Figure 20. The axial load ratio is axial load divided by the working load. The axial load decreased after tunnelling because the degradation of bearing capacity of the pile and the extent of loss of bearing capacity depends on the degree of volume loss. To maintain the equilibrium of loads, the base resistance is transferred to the pile shaft so that positive skin friction along the pile increases. If the extra positive skin friction cannot compensate for the unavoidable large degradation of end bearing capacity, a larger pile settlement would be predicted.

It should be noticed that there was a short part of the pile with the negative friction at the pile tip after tunneling. One scenario about it is that it indicated the stress relief at that area. Because of the drag load, axial load also increased at the tip of the pile. However, the possibility of error generated during

the modelling cannot be eliminated with limited models. It should be tested in more refined model and to see the behavior of the pile.

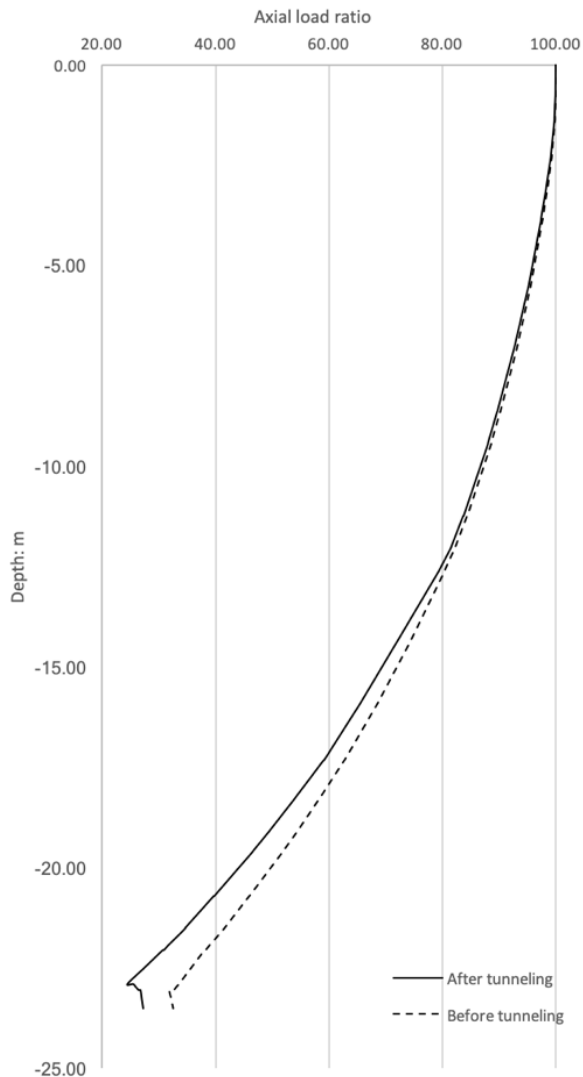


Figure 19. Change of axial load of the pile in deep tunnel model

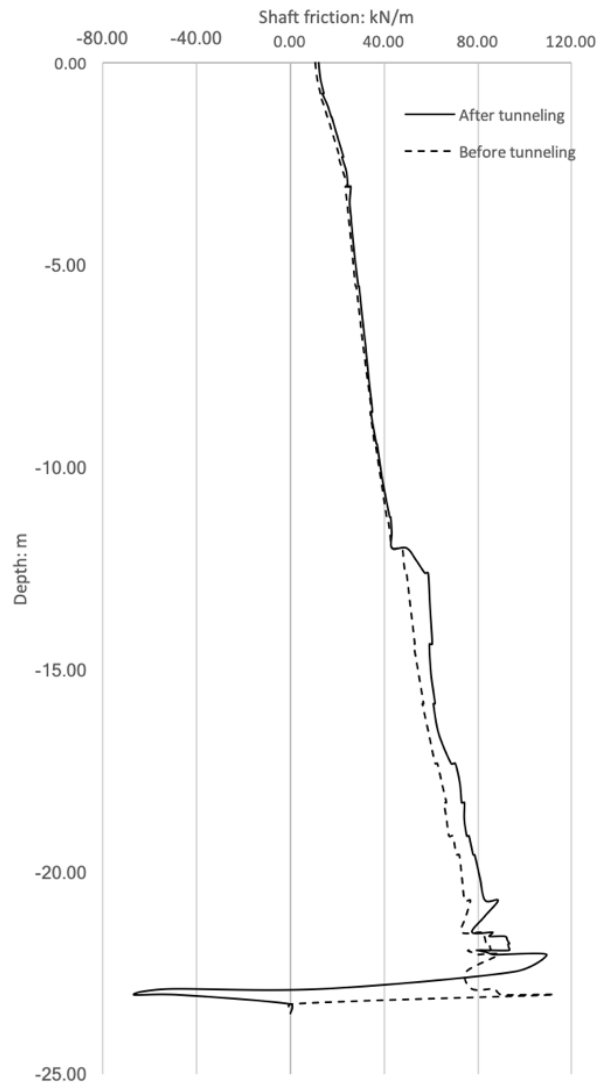


Figure 20. Change of Shaft friction of the pile in deep tunnel model

5.3.2..2 Pile movement

Figure 21 illustrates the pile tip settlement during the MTBM advancement procedure. One thing should be emphasized ahead that relative distance in Figure 21 describes the distance between the bore front of the machine and the plane where the pile located. Zero means the cutting face of the MTBM is exactly beneath the pile axis. In this way, the relationship between the pile settlement and the MTBM advancement can be more visualized.

As illustrated in Figure 21, there was a neglectable settlement less than 1mm before the machine arrived the plane where the pile located. During the phase of MTBM, only a small settlement less than 2 mm was induced. It is mainly because the size of the MTBM was relatively small and the contraction of the shield was deactivated in the case of MTBM. After the MTBM passed, an abrupt

increase of settlement, up to 7mm, happened during lubrication phase, where the contraction happened under smaller lubrication pressure compared with overburden pressure. When final linings were erected, the settlement was held at a stable level. With volume loss of 3%, the pile tip settled 8mm due to micro-tunnelling procedure and 65% of the total settlement happened during the lubrication phase.

5.3.2..3 The variation of base load

The change of base load during the excavation procedure was illustrated in Figure 22. Base load ratio is the ratio between the base load at the tip and the working load at the pile head. Combined Figure 21 and Figure 22 together, one basic rule can be concluded which is the degradation of base resistance induced the pile settlement. The drop of base load ratio mainly happened at lubrication phase, from 33% to 27%. It is coincident with the abrupt decrease of the pile tip settlement. At the lining phase, a slight increase of the base load was observed. It is because that the negative skin friction at bottom of the pile was generated due to stress relief at shown in Figure 20. Besides, the little fluctuation at the beginning of lubrication phase was caused by the system error of curve generation and it cannot represent the pile behaviour.

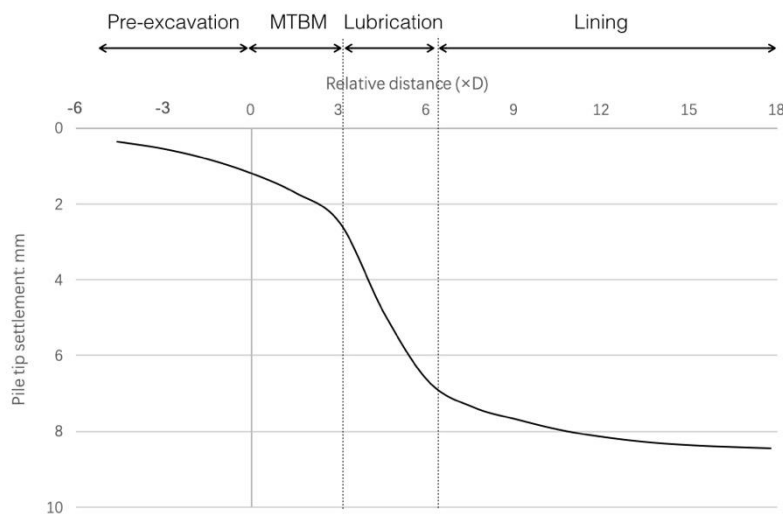


Figure 21. Change of pile tip settlement of the pile during deep MTBM advancement

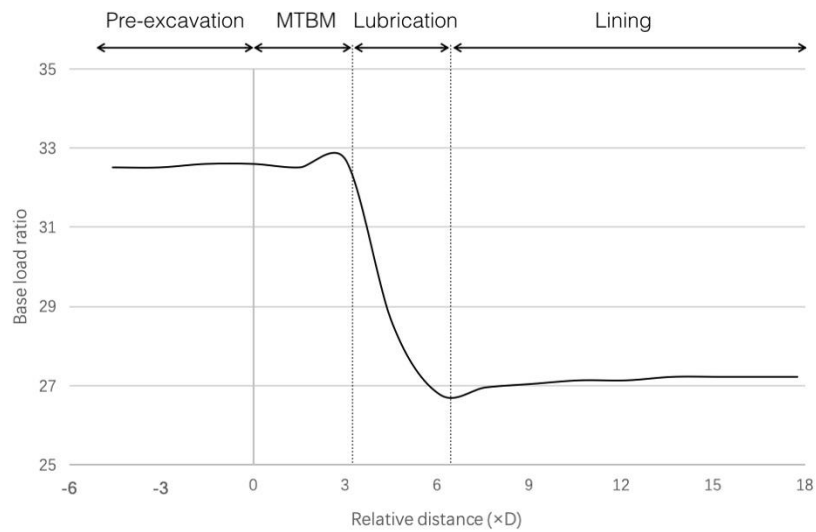


Figure 22. Change of base load of the pile during deep MTBM advancement

5.3 Shallow tunnel

5.3.1 Geometry

The geometry of the shallow tunnelling model is illustrated in Figure 23. All parameters are the same with the deep tunnel model except the length of pile, namely L_2 , is 40m.

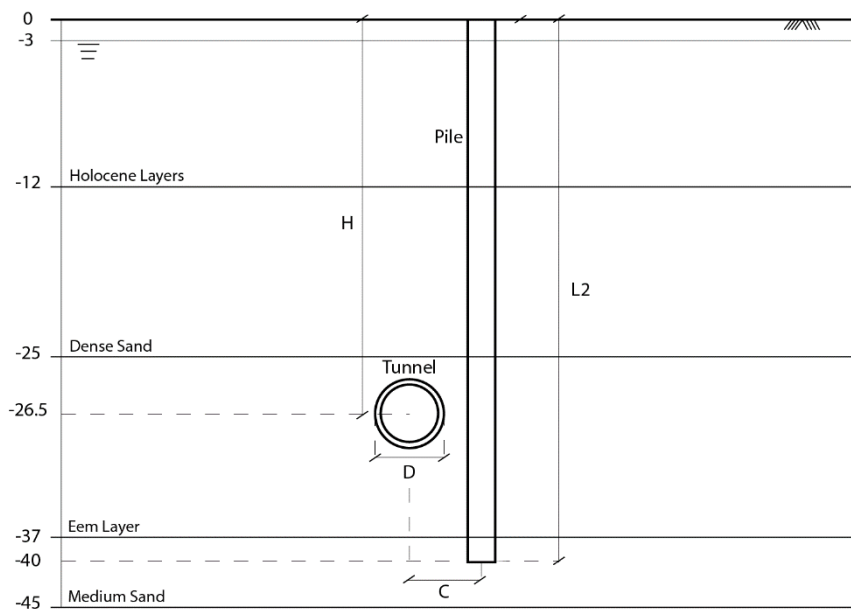


Figure 23. Sketch of the configuration of the shallow tunnel model

5.3.2 Pile responses due to tunnelling

5.2.3..1 Load transfer mechanism

In the shallow tunnelling model, changes in the axial load and shaft friction were illustrated in Figure 24 and Figure 25. The variation of bending moment and pile lateral movement due to tunnelling were

recorded in Figure 26 and Figure 27. The bending moments are treated as positive if they act to bend the pile away from the tunnel.

The pile can be divided into two parts based on its behaviour, one is above the micro-tunnel axis and another part is below the micro-tunnel. The stress relief due to tunnelling causes negative skin friction to act along the pile shaft above the tunnel level. To maintain the equilibrium, the pile shaft below the tunnel level (which can be seen as a fixed end) would support the drag-load from the upper part so that positive skin friction increases. Only when the positive shaft resistance and pile base are fully mobilized, the settlement would become a problem.

Compared with the settlement, shallow tunnelling procedure had significant influence on the distribution of the bending moment along the pile. There was a trend of moving toward the tunnel for the pile at the level of the tunnel horizontal axis.

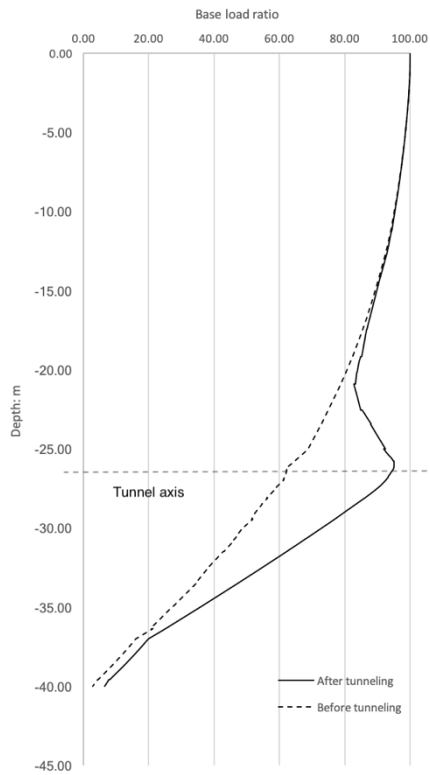


Figure 24. Change of base load of the pile in the shallow tunnelling model

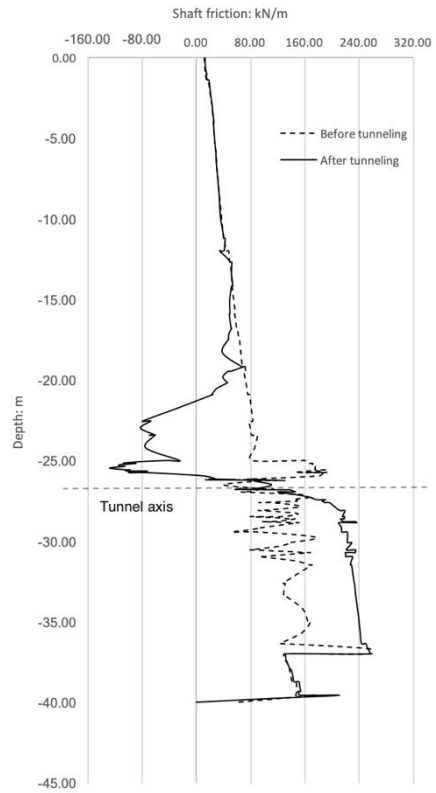


Figure 25. Change of shaft friction of the pile in the shallow tunnelling model

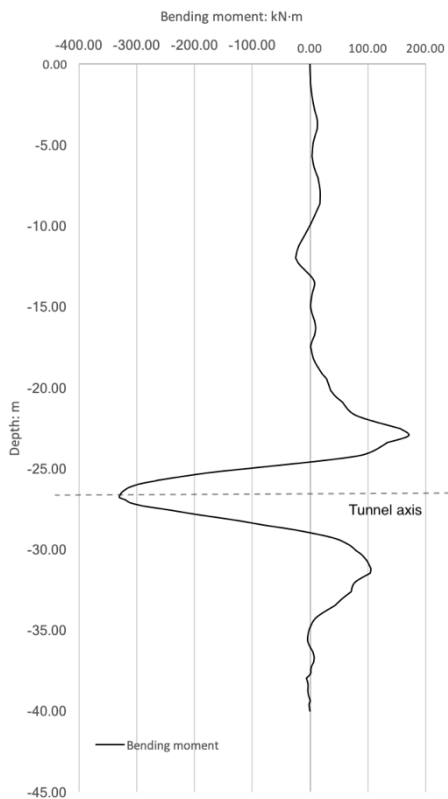


Figure 26. Bending moment of the pile due to tunnelling in the shallow tunnelling model

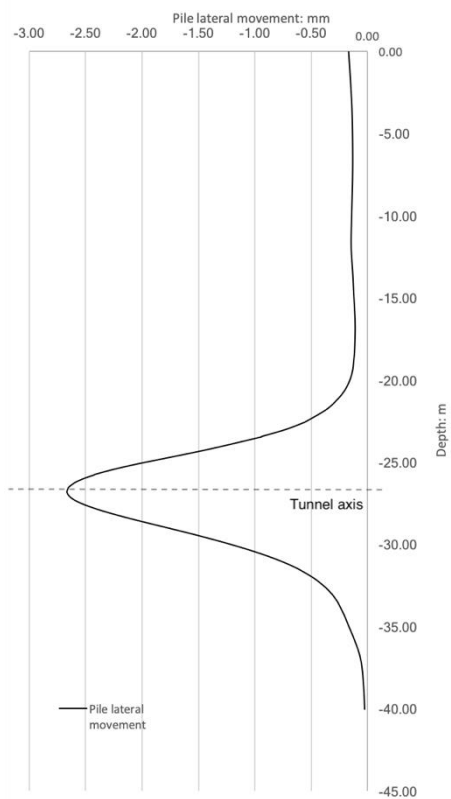


Figure 27. Lateral movement of the pile due to tunnelling in the shallow tunnelling model

5.2.3..2 Pile movement

As shown in Figure 28, in the shallow tunnelling model, the gradient of the pile tip settlement kept the same for the MTBM phase and the lubrication phase. No significant settlements occurred during the whole procedure. The total settlement stopped at 4mm after linings were erected.

On the other hand, the response of the long pile concerning the base load was different from the case of the short pile. As shown in Figure 29, an increase of base load was observed after tunnelling, indicating that the total shaft friction decreased after the tunnelling process. In this case, the pile settlement was induced by the stress relief of shaft resistance rather than base resistance.

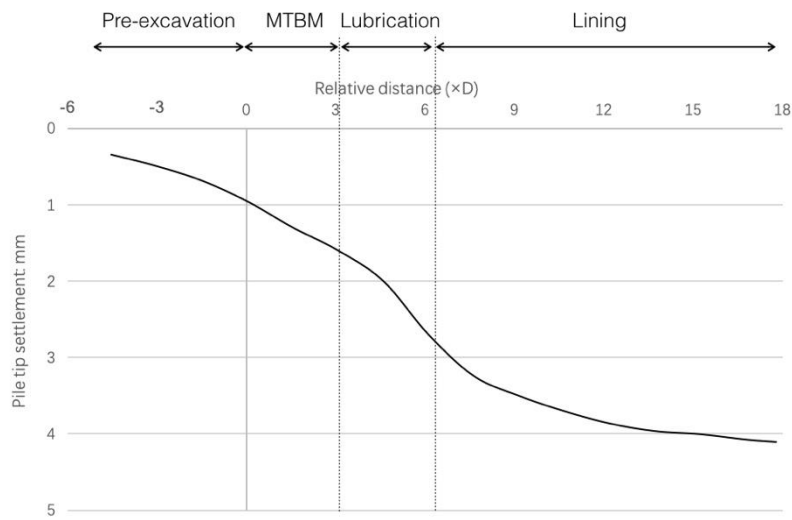


Figure 28. Change of base load of the pile during shallow MTBM advancement

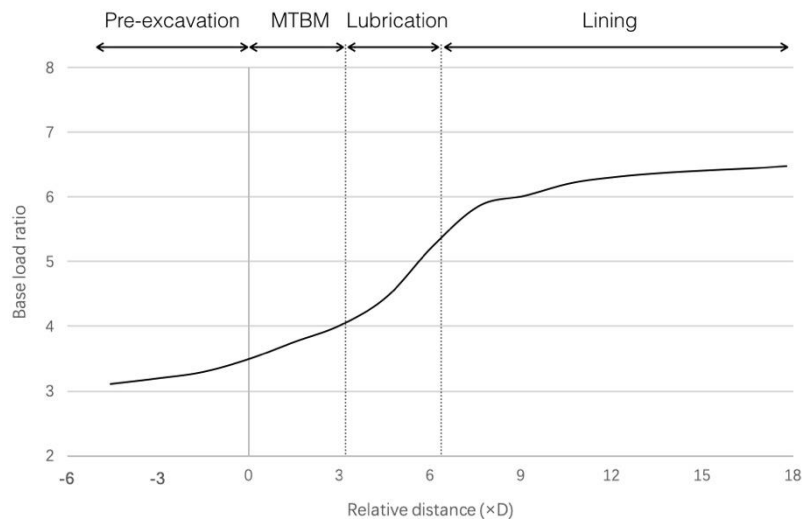


Figure 29. Change of pile tip settlement during shallow MTBM advancement

5.4 Different failure mechanisms of deep and shallow tunnelling models

Based on different responses of piles due to the micro-tunnelling procedure, it is reasonable to conclude that failure mechanisms for these two models are also different. For the deep tunnelling model, the pile underwent a significant settlement due to the stress relief of the base resistance at the volume loss of 3%, which represents the real situation when the specific MTBM machine is used. With the growth of volume loss, the degradation of the base resistance becomes worse. When the threshold of volume loss is exceeded, the pile failure due to large settlement can be expected.

For the shallow tunnelling model, generation of the negative skin friction along the shaft above the tunnel level force the positive friction and the base load to increase. Only when the positive shaft resistance and pile base are fully mobilized, the settlement would become a problem. However, the distribution of the bending moment along the pile at large volume loss should be paid special attention especially at the maximum bending moment as has been suggested in the study of Mroueh and Shahrour (2002).

6 Parametric study

According to two 3D models, basic knowledge about pile-tunnel interaction mechanisms had been established. For a better understanding of the problem, some parametric studies based on deep tunnel model were conducted in PLAXIS 2D.

6.1 Influence zone

In the study of Selemetas et al. (2005), an influence zone based on pile head relative settlement was proposed as shown in Figure 30, inside of which the potential of settling more than the ground surface for piles exists when volume losses exceed a threshold value.

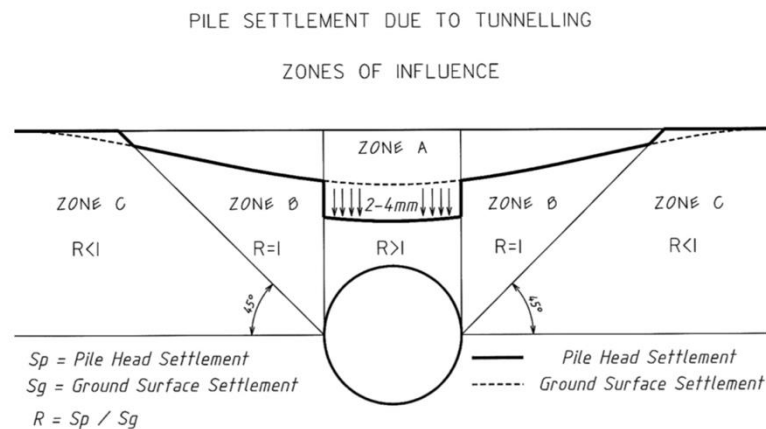


Figure 30. Influence zone proposed by Selemetas et al. (2005) based on pile head relative settlement

A parametric study about influence zone was exerted in this research with single piles installed at different locations near the micro-tunnel. There were three groups of tests, namely Group A, B and C and each group included 19 tests with same volume loss but different pile conditions. Details of the tests were listed in Table 18 and locations of 19 pile toes were illustrated in Figure 31. A similar influence zone was proposed concerning stress relief of the pile and pile failure but there were several distinctions compared with the study of Selemetas et al. (2005).

Pile responses with three different volume loss were interpreted separately. At a small degree of volume loss, similar boundary lines like the lines in Figure 30, dividing pile behaviours concerning pile head relative settlement were found. As volume loss increased, the pile failure occurred for those piles located close to the micro-tunnel. Based on pile failure, a critical zone inside the influence zone was defined. For piles out of the critical zone, the possibility of pile failure is neglectable regardless of the volume loss. In this way, an integrated influence zone including three subdivided areas was established.

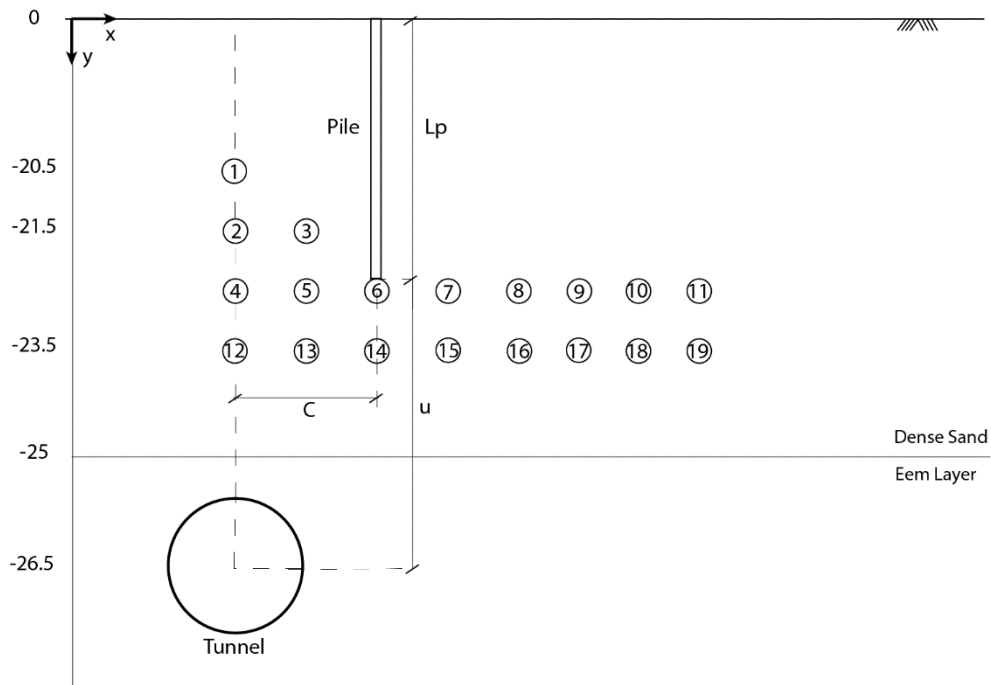


Figure 31. Locations of 19 pile toes

Table 18. Test arrangement and test conditions

Test No.	Coordinate (x, y) (m)	Embedment depth, L_p (m)	Normalized horizontal clearance C/D	Normalized vertical distance u/D	Working load (kN)	Volume loss (%)		
						A	B	C
P1	(0, -20.5)	20.5	0	3	955			
P2	(0, -21.5)	21.5	0	2.5	1015			
P3	(1, -21.5)	21.5	0.5	2.5	1015			
P4	(0, -22.5)	22.5	0	2	1075			
P5	(1, -22.5)	22.5	0.5	2	1075			
P6	(2, -22.5)	22.5	1	2	1075			
P7	(3, -22.5)	22.5	1.5	2	1075			
P8	(4, -22.5)	22.5	2	2	1075			
P9	(5, -22.5)	22.5	2.5	2	1075			
P10	(6, -22.5)	22.5	3	2	1075	3	9	15
P11	(7, -22.5)	22.5	3.5	2	1075			
P12	(0, -23.5)	23.5	0	1.5	1135			
P13	(1, -23.5)	23.5	0.5	1.5	1135			
P14	(2, -23.5)	23.5	1	1.5	1135			
P15	(3, -23.5)	23.5	1.5	1.5	1135			
P16	(4, -23.5)	23.5	2	1.5	1135			
P17	(5, -23.5)	23.5	2.5	1.5	1135			
P18	(6, -23.5)	23.5	3	1.5	1135			
P19	(7, -23.5)	23.5	3.5	1.5	1135			

6.1.1 Pile responses at volume loss of 3%

Based on the parameters of AVN1600AB-standard MTBM provided by HERRENKNECHT Company, a volume loss of 3% will be generated in real micro-tunnel excavation activities. The first group of tests were set to simulate this real micro-tunnel excavation condition.

6.1.1.1 Changes in bearing loads of piles

The changes of bearing loads of 19 tests were listed in Table 19. Firstly, results of two groups of piles, namely P4 – P11 with the length of 22.5m and P12 – P19 with the length of 23.5m, were selected to investigate the impact of horizontal clearance on bearing load. Normalized bearing loads of these two groups were illustrated in Figure 32, where normalized bearing load is the ratio that the base load after tunnelling divided by the initial base load before tunnelling.

In Figure 32, the relaxation of base capacity was relieved as the pile located farther from the tunnel. When the pile tip exceeded a specific boundary, where normalized bearing load value was zero, the base load reversely increased after the tunnelling. Based on this character, a boundary line could be illustrated as shown in Figure 33 which divides two load transfer mechanisms. Inside the zone, the bearing load decreased after tunnelling activities due to the stress relief of the base resistance. Outside the zone, the bearing load increased after tunnelling to compensate for the decrease of the shaft resistance.

Table 19. Variations of bearing loads of 19 piles with volume loss of 3%

Test No	Base load ratio (%)		Normalized bearing load	Test No	Base load ratio (%)		Normalized bearing load
	Before tunnelling	After tunnelling			Before tunnelling	After tunnelling	
P1	46,33	44,04	0,95	P11	45,71	48,98	1,07
P2	45,26	41,38	0,91	P12	41,11	32,81	0,80
P3	45,69	41,38	0,91	P13	41,11	33,20	0,81
P4	43,67	37,96	0,87	P14	41,90	35,57	0,85
P5	43,67	38,78	0,89	P15	41,50	38,34	0,92
P6	43,67	40,00	0,92	P16	42,29	42,69	1,00
P7	44,08	40,41	0,92	P17	42,29	44,66	1,06
P8	42,86	41,22	0,96	P18	41,50	45,06	1,09
P9	45,31	46,53	1,03	P19	41,90	46,64	1,11
P10	44,90	47,35	1,05				

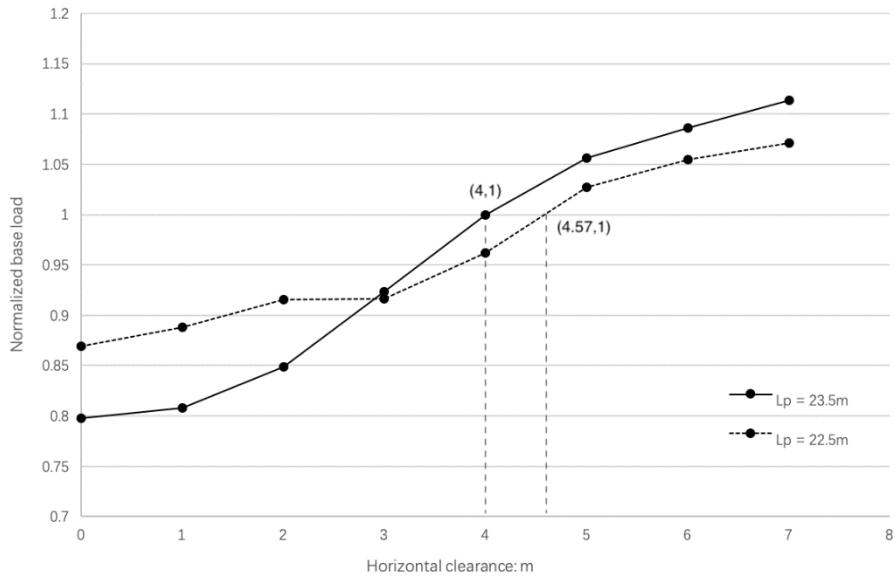


Figure 32. Changes of base loads of P4 – P19 with volume loss of 3%

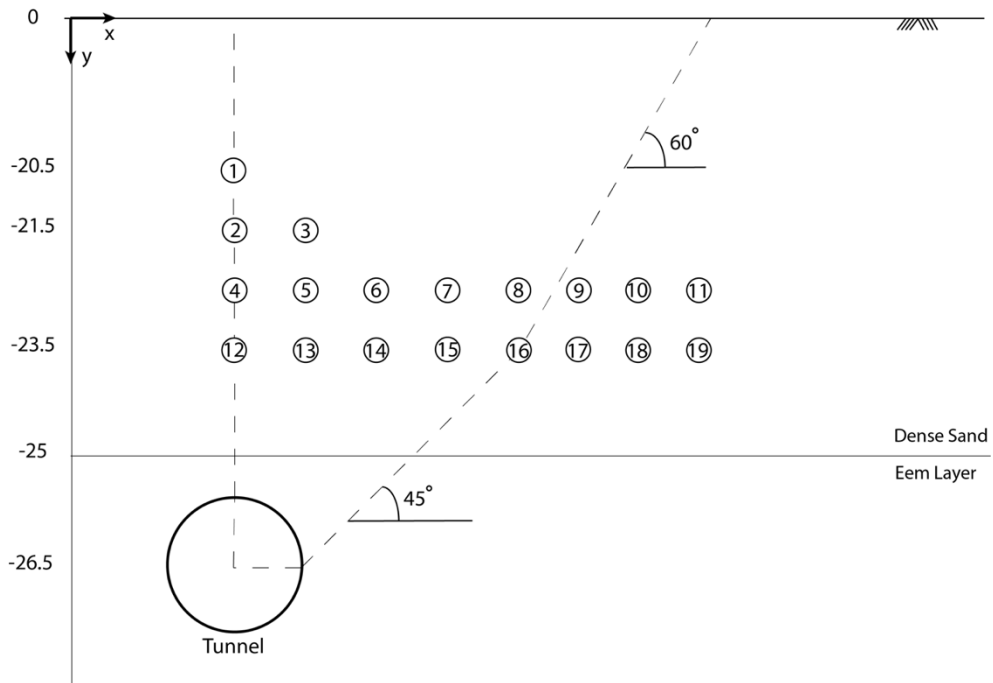


Figure 33. The first boundary of the influence zone

6.1.1.2 Pile head settlement

Pile head settlements of P4 to P19 were illustrated in Figure 34 and details of pile head relative settlements were listed in Table 20. Pile settled in the same trend of the subsurface soil movement and all piles settled in the range of 4mm and 9mm. The maximum pile head relative settlement was 2mm for P12 and P13. The neglectable relative settlements indicated that no pile failure happened with volume loss of 3%.

In the field monitoring report proposed by Cook et al. (2007), background settlements at Station-Rokin and Station Ceintuurbaan over a period of 4 years were measured by extensometer as shown in Figure 35 and Figure 36. At the end of measurement, accumulated surface settlement at two stations were 6.4mm and 8.8mm, respectively. The corresponding building settlements given in the report were 5.2mm and 8mm. Compared with these field measurements, it is reasonable to say that the condition of micro-tunnelling with the volume loss of 3% could only induce limited damage to the buildings at Asmterdam.

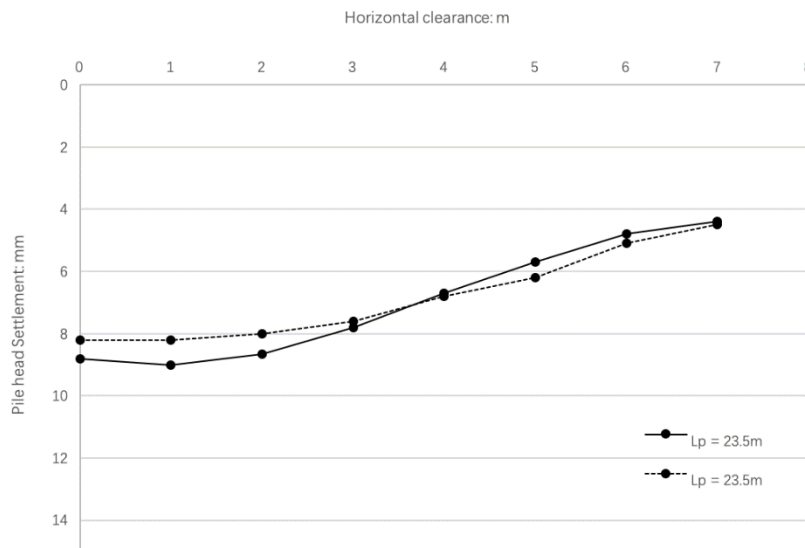


Figure 34. Pile head settlements of P4-P19 with volume loss of 3%

Table 20. pile head relative settlements of P4-P19 with volume loss of 3%

Test No	Pile head relative settlement (mm)	Test No	Pile head relative settlement (mm)
P1	-1	P11	0
P2	-1,1	P12	-1,98
P3	-1,1	P13	-2
P4	-1,5	P14	-1,7
P5	-1,5	P15	-1,2
P6	-1,3	P16	-0,7
P7	-1,1	P17	-0,3
P8	-0,7	P18	0
P9	-0,5	P19	0,15
P10	0		

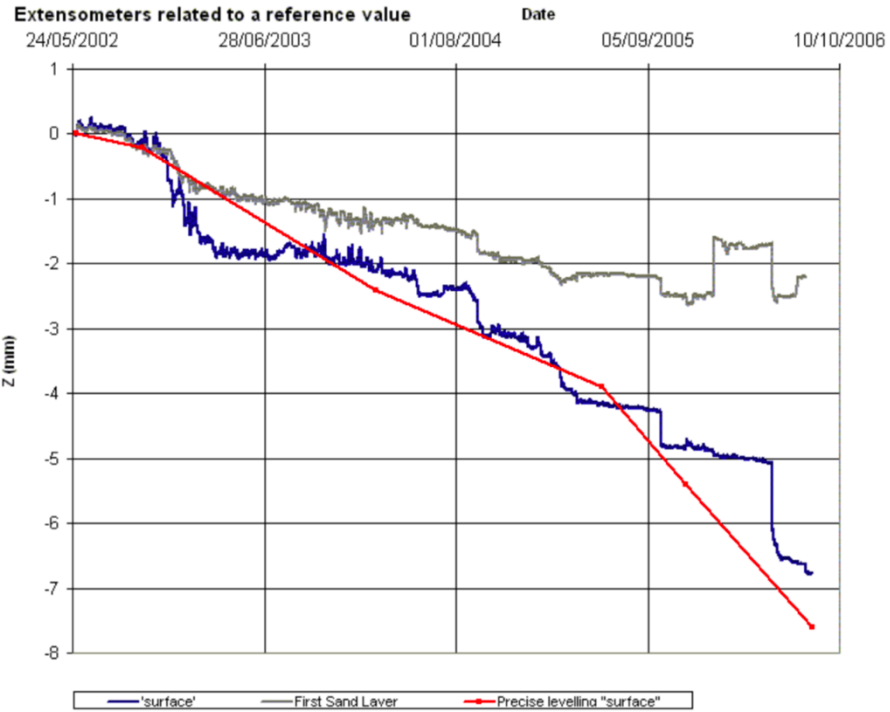


Figure 35. Extensometer readings related to a reference value at Station-Rokin

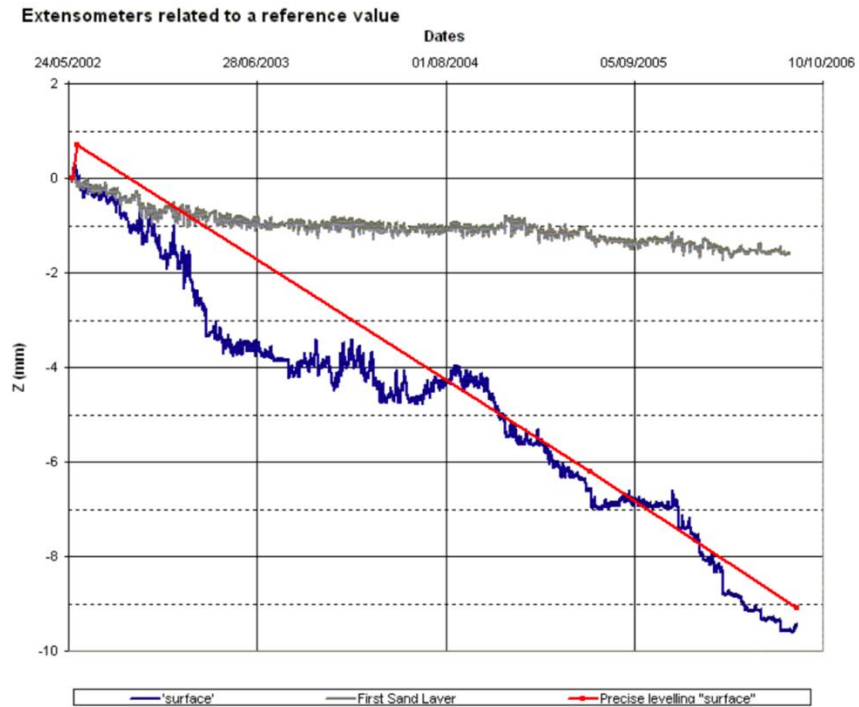


Figure 36. Extensometer readings related to a reference value at Station-Ceintuurbaan

6.1.2 Pile responses at volume loss of 9%

Because of the relatively small diameter of MTBM, there is hardly any large settlement or relative settlement happened under the real excavation condition. To get more information about the influence zone and pile responses due to tunnelling, the volume loss was increased to 9% for the second group of tests.

6.2.1..1 Changes in bearing loads of piles

The changes of normalized bearing loads under volume loss of 9% were illustrated in Figure 37. It is found that the position of the boundary line did not change as the volume loss increased from 3% to 9%. It is reasonable to believe that this line is not influenced by the degree of volume loss. This scenario will be affirmed in the next chapter. Besides, there is one thing should be noticed that for P12 and P13, the normalized base loads were the same, which means their full bearing capacities were mobilized and failure happened at P12 and P13. The failure can be more visualized from the view of pile head relative settlement and it will be given later.

Table 21. Changes of base loads of 19 piles with volume loss of 9%

Test No	Bearing load ratio (%)		Normalized bearing load	Test No	Bearing load ratio (%)		Normalized bearing load
	Before tunnelling	After tunnelling			Before tunnelling	After tunnelling	
P1	46,33	41,28	0,89	P11	45,71	52,65	1,15
P2	45,26	36,64	0,81	P12	41,11	25,30	0,62
P3	45,69	35,78	0,78	P13	41,11	25,30	0,62
P4	43,67	28,57	0,65	P14	42,29	29,64	0,70
P5	44,49	30,61	0,69	P15	41,50	35,97	0,87
P6	43,67	33,06	0,76	P16	42,29	42,29	1,00
P7	44,08	36,73	0,83	P17	42,29	45,85	1,08
P8	42,86	39,59	0,92	P18	41,50	47,83	1,15
P9	45,31	47,35	1,05	P19	41,90	50,99	1,22
P10	44,90	49,39	1,10				

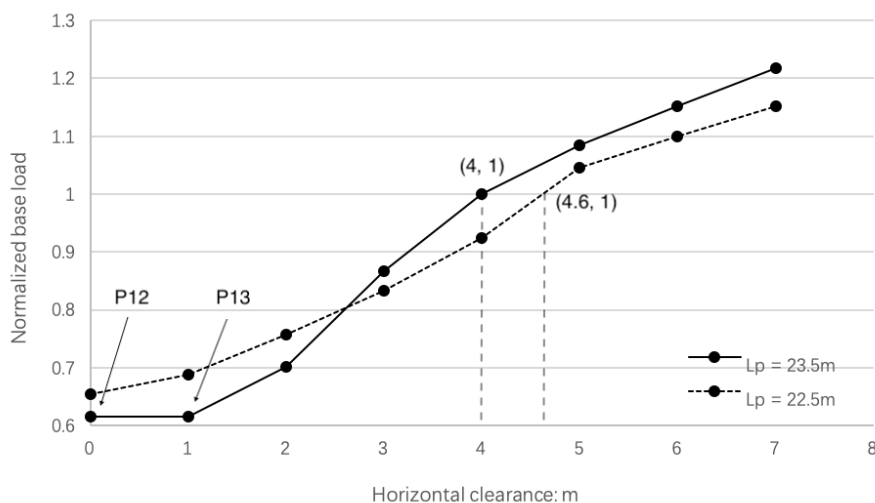


Figure 37. Variation of base loads of P4-P19 with volume loss of 9%

6.2.1..2 Pile head settlement

Figure 38 shows the pile head settlements of piles with lengths of 22.5m and 23.5m. For the pile with the length of 23.5m, when the horizontal clearance less than 2m (1D), there were abrupt increases of pile head settlements with volume loss of 9%, indicating the pile failure. This is mainly because the full bearing capacities of P12 and P13 had been mobilized and large relative settlement happened, as shown in Figure 39. Besides, P14 also had a trend to fail if the volume loss kept increasing.

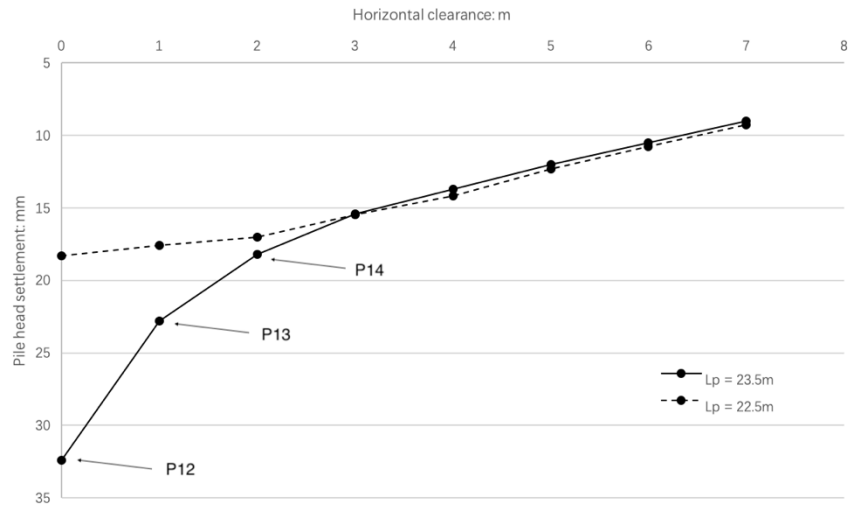


Figure 38. Pile head settlements of P4-P19 with volume loss of 9%

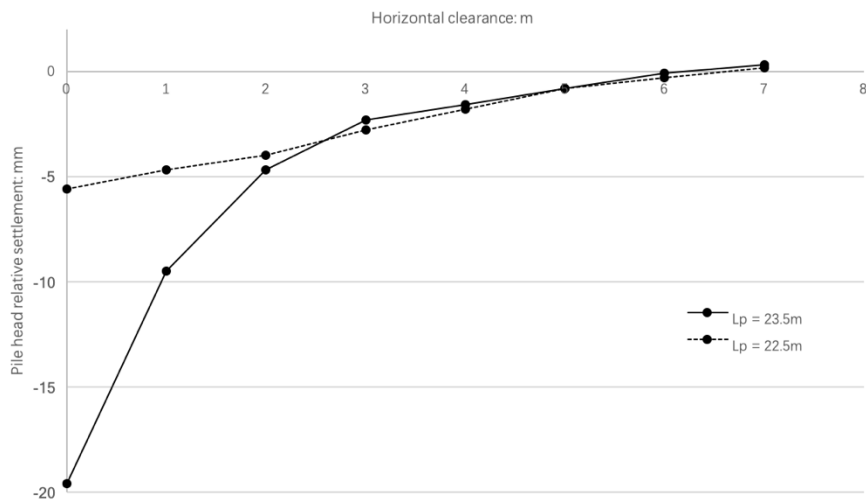


Figure 39. Pile head relative settlements of P4-P19 with volume loss of 9%

6.1.3 Pile responses at volume loss of 15%

Volume loss of 15% is nearly the maximum value that the model could reach before the tunnel collapsed. It seems unrealistic but was adopted to test the pile behaviour in extreme conditions.

6.3.1.1 Changes in bearing loads of piles

As what have done for previous two groups, changes of normalized bearing loads were illustrated in Figure 40. There are two things should be noticed. First, the boundary of the influence zone kept the same position. It means that for a specific embedded ratio of micro-tunnel, there is a fixed boundary which divides two pile load transfer mechanisms regardless of volume loss. This boundary line was used to establish the influence zone of the micro-tunnelling.

Second, at extreme large volume loss, P4, P5 and P6 showed the same responses as P12, P13 and P14, respectively. P12, P13 and P14 are piles that failure had occurred at volume loss of 9%. Based on the behaviours of these 6 piles, it is believed that inside the influence zone, there is a smaller area that potential for pile failure exists when volume losses exceed a threshold value. Outside the area, even though piles might undergo the relaxation of bearing capacity, the possibility of pile failure can be neglected regardless of the volume loss. Therefore, a critical zone ‘Zone A’ was identified as shown in Figure 41.

Table 22. Changes of base loads with volume loss of 15%

Test No	Bearing load ratio (%)		Normalized bearing load	Test No	Bearing load ratio (%)		Normalized bearing load
	Before tunnelling	After tunnelling			Before tunnelling	After tunnelling	
P1	46,33	36,24	0,78	P11	43,67	51,02	1,17
P2	45,26	28,45	0,63	P12	41,11	41,11	0,62
P3	45,69	28,45	0,62	P13	41,11	41,11	0,62
P4	43,67	27,76	0,64	P14	41,90	41,90	0,65
P5	44,49	27,76	0,62	P15	41,50	41,50	0,90
P6	43,67	28,57	0,65	P16	42,29	42,29	1,00
P7	44,08	34,69	0,79	P17	42,29	42,29	1,15
P8	42,86	37,96	0,89	P18	41,50	41,50	1,22
P9	45,31	48,57	1,07	P19	41,90	41,90	1,32
P10	44,90	51,43	1,15				

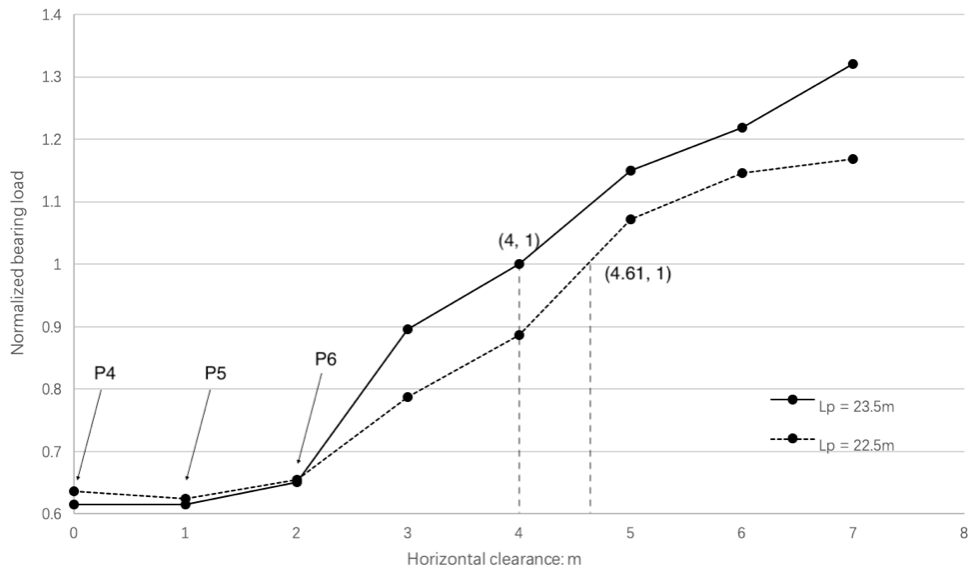


Figure 40. Changes of base loads of P4-P19 with volume loss of 15%

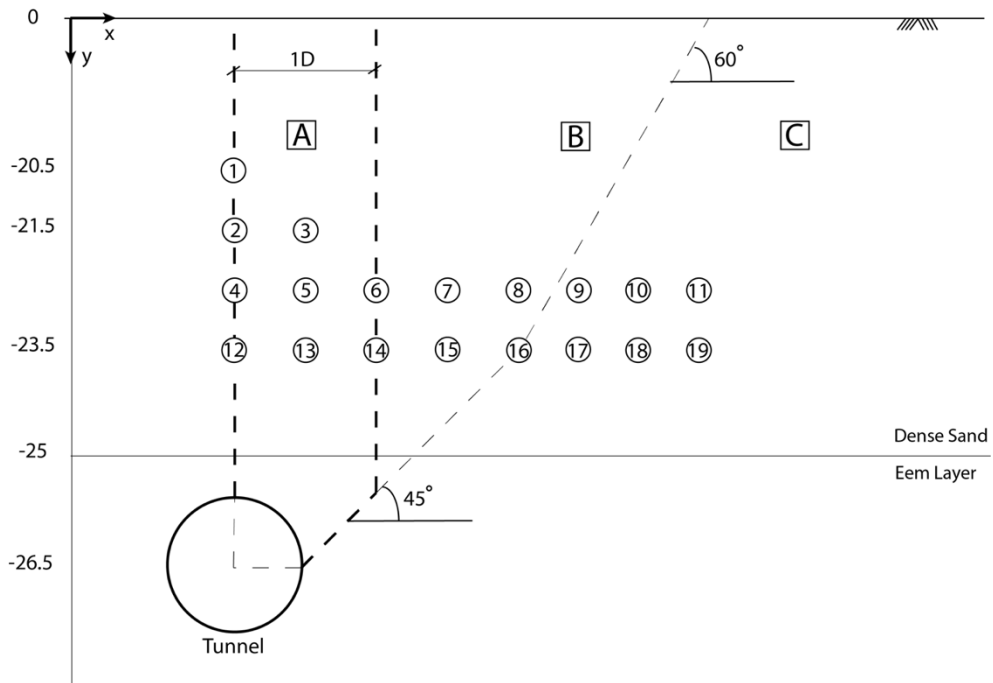


Figure 41. Three subdivided parts of the influence zone

6.1.4 Influence zone in the vertical direction

Previous chapters discuss the impact of horizontal configuration on pile responses due to tunnel. A boundary line and a critical zone were defined. To figure out the impact of micro-tunnelling and the range of the induced influence zone in the vertical direction, five piles were chosen as shown in Figure 42 and the volume loss continuously increased from 0 to 15%. The pile head relative settlements were recorded with the increase of volume loss as shown in Figure 43.

As illustrated in Figure 43, P2, P12 and P13 experienced large relative settlements at pile head, which represented the mobilization of full bearing capacities of piles. Besides, the closer the pile tip and the tunnel were, the smaller the volume loss that the tunnel can reach before pile failure. For P1 and P15, no significant signal of failure happened until volume loss of 15%. Based on the same criterion of failure, the area where P1 located was marked as a relatively safe zone, just like where P15 was.

Based on the whole study mentioned above, an integrated influence zone around the micro-tunnel was built as shown in Figure 44.

6.1.5 Influence zone of micro-tunnel

As shown in Figure 44, an influence zone of micro-tunnel concerning the impact on adjacent piles was established based on several parametric studies. The whole area was divided into three parts marked as Zone A, Zone B and Zone C. For piles located in Zone A, failure regarding large pile head relative settlement could occur when the volume loss exceeds a threshold value and the impact of micro-tunnelling was more significant as the pile is located closer to the micro-tunnel. Therefore, Zone A is also called as the critical area. In Zone B, base loads of piles decreased after the micro-tunnel excavation because of the relaxation of base capacity, but failure was rarely seen regardless of the volume loss. In zone C, base loads of piles increased after tunnelling because of the stress relief of shaft capacity as surrounding soil moving towards the micro-tunnel.

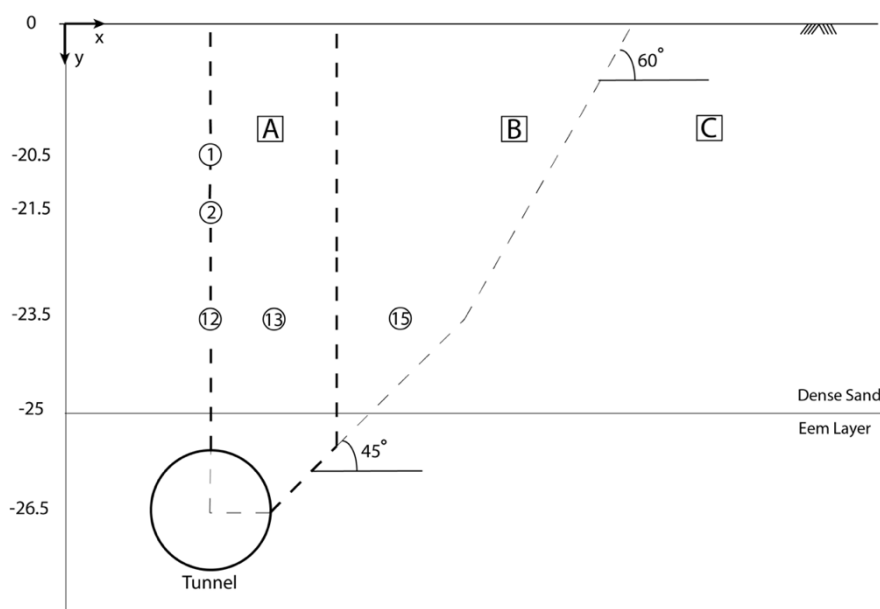


Figure 42. Five pile tests to figure out the vertical boundary of the influence zone

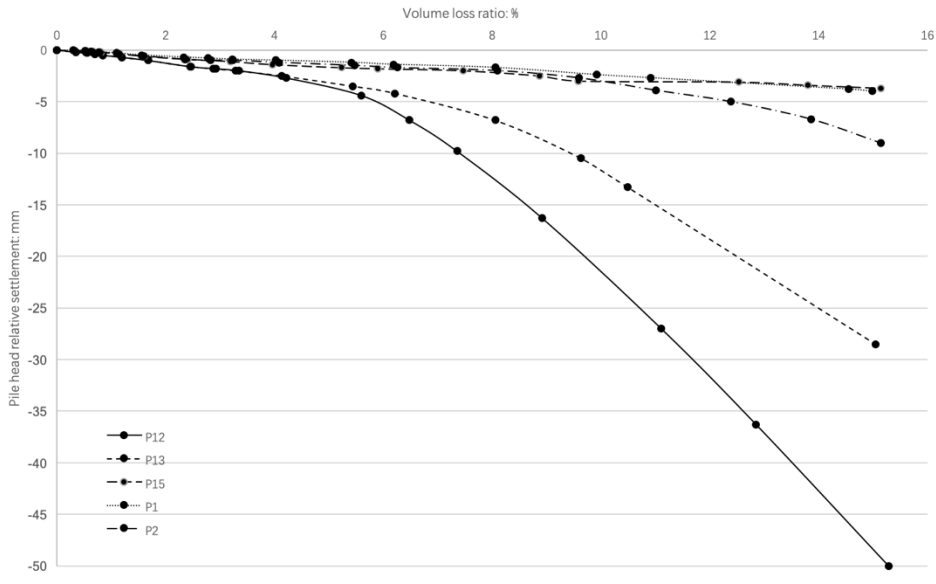


Figure 43. Pile head relative settlements with increasing volume loss

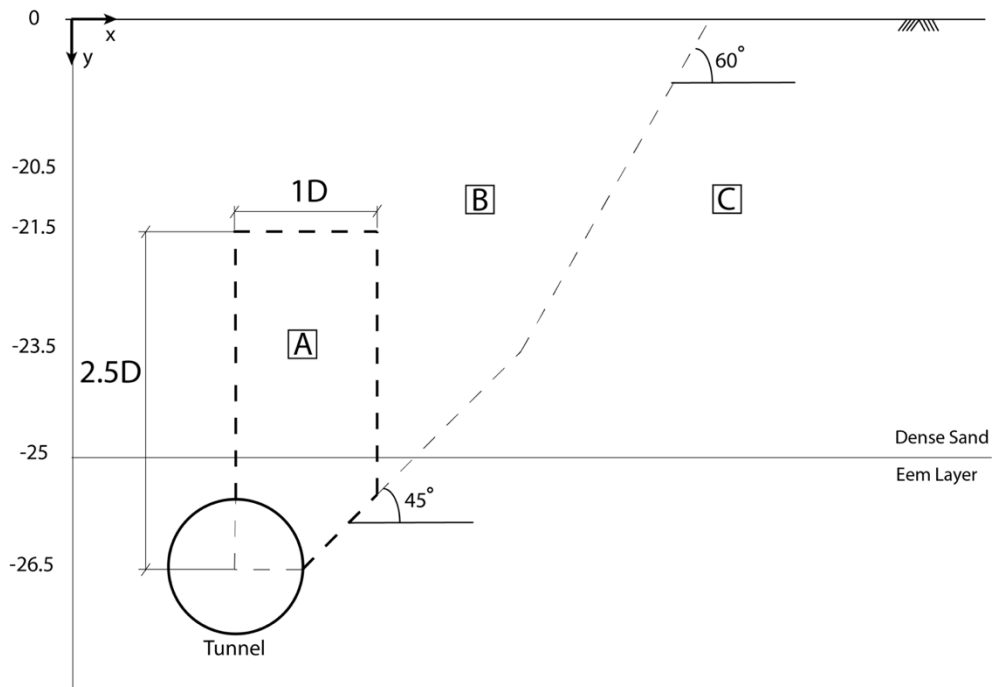


Figure 44. An integrated influence zone of MTBM

6.2 The impact of micro-tunnelling on bearing capacity of the pile

The problem of bearing capacity has been mentioned several times when other questions were discussed. An influence zone concerning stress relief of piles was also proposed in the last Section 6.1.5. This section summarizes all aspects about bearing capacity mentioned before and a comprehensive understanding of the problem is given.

6.2.1 The change of bearing load during the MTBM advancement procedure

Mechanisms of load transfer of pile can be divided into two types corresponding to relative micro-tunnel depth compared to pile length. In this research, they were called ‘deep tunnelling’ model and ‘shallow tunnelling’ model.

6.1.2..1 Deep tunnelling model

‘Deep tunnelling’ refers to the cases where the pile tip is located close to and above the micro-tunnel. Due to micro-tunnel excavation, there is an obvious drop of base load with increasing volume loss because of the relaxation of soil under the pile tip. To maintain the equilibrium, the shaft friction has to increase to compensate for the loss of capacity, which leads to the settlement of the pile. Once the full shaft capacity is mobilized, abrupt settlements happen, and the pile fails with little warning.

For the specific case, as shown in Figure 22, a drop of base load occurred when lubrication phase was passing the plane where the pile was located. It is because the volume loss mainly happened at lubrication phase in the deep tunnelling model.

6.1.2..2 Shallow tunnelling model

On the other hand, for the case of shallow tunnelling, the pile tip is located away from the micro-tunnel or below the micro-tunnel. For long piles, shaft friction supports the main part of working loads, so the base load is relatively small. During micro-tunnel excavation, the positive skin friction of pile decreases in the upper part and increases in the lower part. As a result, an overall reduction in positive skin friction and an increase of base load with increasing volume loss. Only small pile settlements were observed in shallow tunnelling model.

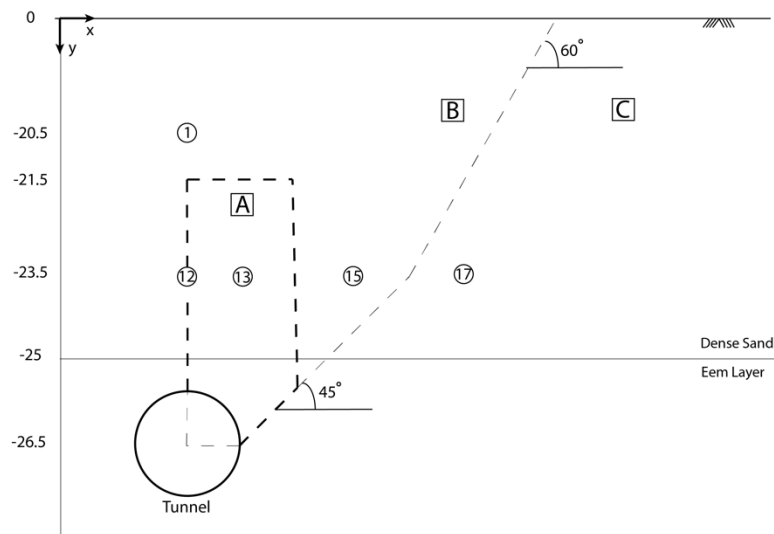


Figure 45. Five pile bearing capacity tests

6.2.2 The changes in bearing loads with increasing volume loss

As shown in Figure 45, five piles (P1, P12, P13, P15 and P17) were selected and their normalized base loads were recorded with the increase of volume loss as illustrated in Figure 46, where the normalized base load is the base load after micro-tunnelling divided by the initial value before tunnelling. Due to different locations of piles, five tests showed diverse responses of bearing load due to tunnelling.

6.2.2.1 P12 & P13

These two tests can be classified into one group based on pile responses. For P12, the base load decreased with increasing volume loss and after volume loss exceeded 6%, the base load kept constant. Combined with pile head relative settlement illustrated in Figure 43, it is shown that the full bearing capacity of the pile had been mobilized at volume loss of 6% and obvious relative settlement indicated that pile failure occurred. For P13, failure was also observed at a volume loss of 8%.

6.2.2.2 P15

Contrasted with P12 & P13, the decrease of base load of P15 stopped earlier. The base load decreased to approximately 90% of the initial value and then kept constant. Besides, a small amount of relative settlement shows that pile did not fail. It is believed that micro-tunnelling can only have limited impact on piles located outside of the critical zone, namely Zone A.

6.2.2.3 P1

P1 was also located out of the critical zone but behaved differently from P15. The base load kept decreasing till maximum volume loss of 15% but no pile failure occurred. The diverse behaviour of piles mainly derived from the different pile tip locations. For P1, pile tip kept influenced by the relaxation of soil beneath it due to tunnelling but the level of degradation of bearing capacity was not large enough to mobilized pile failure. The different responses of P1 and P15 should be demonstrated in more detail in further researches.

6.2.2..4 P17

P17 was located at Zone C and its bearing load increased with increasing volume loss. It conforms to the load transfer mechanism of shallow tunnelling model mentioned in the above chapter.

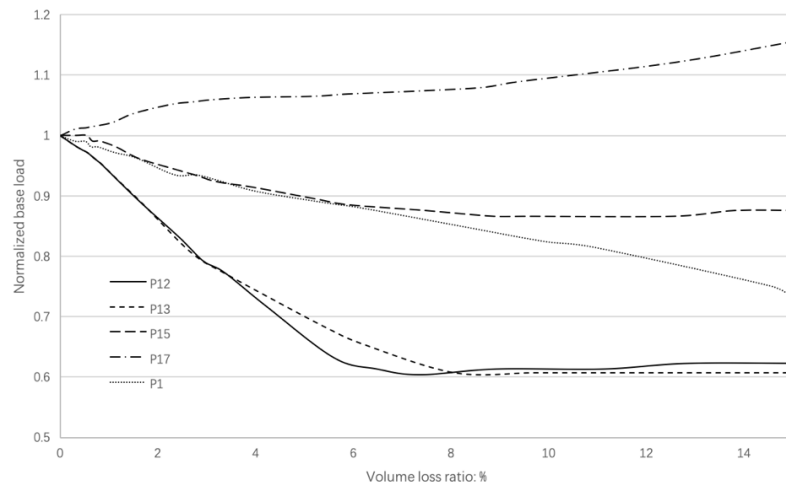


Figure 46. Changes of bearing loads with increasing volume loss

7 Conclusions

Finite element analysis in PLAXIS 3D & PLAXIS 2D were conducted to investigate the impact of micro-tunnelling on pile foundations. Two three dimensional models were built in PLAXIS 3D to simulate the advancement of micro-tunnel with different embedded depth. A series of parametric studies were carried out in PLAXIS 2D to generate pile responses with variable parameters, including volume loss, length of piles and clearance. The following understanding of the research questions has been made from the study:

7.1 Deep and shallow tunnelling models

The problem of interaction between micro-tunnel and adjacent piles can be classified into two categories depending on relative micro-tunnel depth compared to pile length, which are called ‘deep tunnelling’ model and ‘shallow tunnel’ model, respectively. Two models follow different pile load transfer mechanisms and failure criteria. For deep tunnelling condition, there is a critical pile settlement due to the degradation of base resistance and pile head settlement can be used as the criterion of failure. For shallow tunnelling condition, no obvious settlements were observed for piles and attention should be paid more on the change of bending moment of the pile after the micro-tunnelling procedure.

7.2 Influence zone of micro-tunnel

In the model of micro-tunnel, normalized base load and pile head relative settlement were used as criteria to suggest the influence zone around the micro-tunnel. For piles inside the influence zone, base loads decrease with increasing volume because of the loss of base resistance. However, the impact of micro-tunnelling is limited if the clearance increases. Inside the influence zone, a critical zone with a smaller area was verified in which piles have a potential to fail with increasing volume loss. For piles located at the zone belonging to influence zone but out of the critical area, although the decrease of base load was observed, no pile failure occurred with volume loss in ranges considered in this research.

As shown in Figure 44, an influence zone of micro-tunnel concerning the impact on adjacent piles was established based on several parametric studies. The whole area was divided into three parts marked as Zone A, Zone B and Zone C. For piles located in Zone A, failure regarding large pile head relative settlement could occur when the volume loss exceeds a threshold value and the impact of micro-tunnelling was more significant as the pile is located closer to the micro-tunnel. Therefore, Zone A is also called as the critical area. In Zone B, base loads of piles decreased after the micro-tunnel excavation because of the relaxation of base capacity, but failure was rarely seen regardless of the volume loss. In zone C, base loads of piles increased after tunnelling because of the stress relief of shaft capacity as surrounding soil moving towards the micro-tunnel.

8 Reference

- APIRP2A 2006. the American Petroleum Institute
- ATTEWELL, P. B., YEATES, J. & SELBY, A. R. 1986. Soil movements induced by tunnelling and their effects on pipelines and structures.
- BRINKGREVE, R., ENGIN, E. & SWOLFS, W. 2013. Plaxis 3D. *Reference Manual*.
- BRINKGREVE, R., SWOLFS, W., ENGIN, E., WATERMAN, D., CHESARU, A., BONNIER, P. & GALAVI, V. 2018. PLAXIS 3D 2018. *User manual, Plaxis bv*.
- CHEN, L. T., POULOS, H. & LOGANATHAN, N. 1999. Pile responses caused by tunneling. *Journal of Geotechnical and Geoenvironmental Engineering*, 125, 207-215.
- CHENG, C., DASARI, G., CHOW, Y. & LEUNG, C. 2007. Finite element analysis of tunnel–soil–pile interaction using displacement controlled model. *Tunnelling and Underground Space Technology*, 22, 450-466.
- CHIANG, K.-H. & LEE, C.-J. 2007. Responses of single piles to tunneling-induced soil movements in sandy ground. *Canadian Geotechnical Journal*, 44, 1224-1241.
- COB-L520 1999. Richtlijnen Groutdrukmodel. *Technical report, COB, Gouda*.
- COOK, D., DE NIJS, R. & FRANKENMOLEN, S. 2007. Amsterdam Noord/Zuidlijn: Use of Background Monitoring Data Prior to Construction Commencement. *7th FMGM 2007: Field Measurements in Geomechanics*.
- DELFGAAUW, S., BUYKX, S. & BOSCH, J. Jet grout strut for deep station boxes of the north/south metro line Amsterdam: Design and back analysis. Safe Tunnelling for the City and Environment: ITA-AITES World Tunnel Congress, 23-28 May 2009, Budapest, Hungary, 2009. Citeseer.
- JACOBSZ, S., BOWERS, K., MOSS, N. & ZANARDO, G. 2005. The effects of tunnelling on piled structures on the CTRL. *Geotechnical aspects of underground construction in soft ground, Amsterdam*, 115-122.
- JACOBSZ, S., STANDING, J., MAIR, R., HAGIWARA, T. & SUGIYAMA, T. 2004. Centrifuge modelling of tunnelling near driven piles. *Soils and Foundations*, 44, 49-56.
- KAALBERG, F., TEUNISSEN, E., VAN TOL, A. & BOSCH, J. Dutch research on the impact of shield tunnelling on pile foundations. Proceedings of the 5th international symposium on geotechnical aspects of underground construction in soft ground, 2005. Balkema Rotterdam, the Netherlands, 123-131.
- KRAUSE, T. 1987. Schildvortrieb mit flüssigkeits-und erdgestützter Ortsbrust. *Mitteilungen des Instituts für Grundbau und Bodenmechanik der Technischen Universität Braunschweig*.
- LEE, G. T. & NG, C. W. 2005. Effects of advancing open face tunneling on an existing loaded pile. *Journal of Geotechnical and Geoenvironmental Engineering*, 131, 193-201.
- LEE, K., ROWE, R. K. & LO, K. 1992. Subsidence owing to tunnelling. I. Estimating the gap parameter. *Canadian Geotechnical Journal*, 29, 929-940.
- LEE, R. 1994. Deformations caused by tunnelling beneath a piled structure. *Proc. 13th ICSMFE, New Delhi, India*, 873-878.
- LOGANATHAN, N. & POULOS, H. 1998. Analytical prediction for tunneling-induced ground movements in clays. *Journal of Geotechnical and geoenvironmental engineering*, 124, 846-856.
- LOGANATHAN, N., POULOS, H. & STEWART, D. 2000. Centrifuge model testing of tunnelling-induced ground and pile deformations. *Geotechnique*, 50, 283-294.
- MAIR, R., TAYLOR, R. & BRACEGIRDLE, A. 1993. Subsurface settlement profiles above tunnels in clays. *Geotechnique*, 43.
- MAIR, R. & WILLIAMSON, M. The influence of tunnelling and deep excavation on piled foundations. Proceedings of the 8th International Symposium on Geotechnical Aspects of Underground Construction in Soft Ground. Taylor and Francis-Balkema, Seoul, South Korea, 2014. 21-30.

- MARSHALL, A. M. & MAIR, R. J. 2011. Tunneling beneath driven or jacked end-bearing piles in sand. *Canadian Geotechnical Journal*, 48, 1757-1771.
- MARSHALL, M. A. 1998. Pipe-jacked tunnelling: jacking loads and ground movements.
- MORTON, J. & KING, K. Effects of tunneling on the bearing capacity and settlement of piled foundations. *Proc. Tunnelling*, 1979. 57-58.
- MROUEH, H. & SHAHROUR, I. 2002. Three-dimensional finite element analysis of the interaction between tunneling and pile foundations. *International Journal for Numerical and Analytical Methods in Geomechanics*, 26, 217-230.
- NEN9997-1+C2 2017. Geotechnical design of structures - Part 1: General rules.
- SCHANZ, T., VERMEER, P. & BONNIER, P. 1999. The hardening soil model: formulation and verification. *Beyond 2000 in computational geotechnics*, 281-296.
- SELEMETAS, D., STANDING, J. & MAIR, R. The response of full-scale piles to tunnelling. *Proc. of the Fifth Int. Symposium on Geotechnical Aspects of Underground Construction in Soft Ground*, Amsterdam, 2005.
- VERRUIJT, A. & BOOKER, J. 1998. Surface settlements due to deformation of a tunnel in an elastic half plane. *Geotechnique*, 48, 709-713.
- VU, M. N., BROERE, W. & BOSCH, J. 2015. Effects of cover depth on ground movements induced by shallow tunnelling. *Tunnelling and Underground Space Technology*, 50, 499-506.